

1 ***Tissue-autonomous immune response regulates stress signalling during hypertrophy.***

2  
3 Robert Krautz<sup>1#†</sup>, Dilan Khalili<sup>1†</sup>, and Ulrich Theopold<sup>1</sup>

4  
5 <sup>1</sup> Department of Molecular Biosciences, The Wenner-Gren Institute (MBW),  
6 Stockholm University, Svante Arrhenius väg 20C, 114 18 Stockholm, Sweden

7 # *present address:* The Bioinformatics Centre, Department of Biology,  
8 University of Copenhagen, Ole Maaløes Vej 5, 2200 Copenhagen N, Denmark

9 † These authors contributed equally to this work.

10  
11 ***Corresponding authors:*** R. Krautz: [r.krautz@binf.ku.dk](mailto:r.krautz@binf.ku.dk), U. Theopold: [uli.theopold@su.se](mailto:uli.theopold@su.se)

12  
13 ***Abstract***

14  
15 Postmitotic tissues are incapable of replacing damaged cells through proliferation, but need to  
16 rely on buffering mechanisms to prevent tissue disintegration. By constitutively activating the  
17 Ras/MAPK-pathway via *Ras<sup>V12</sup>*-overexpression in the postmitotic salivary glands of  
18 *Drosophila* larvae, we overrode the glands adaptability to growth signals, induced hypertrophy  
19 and stress accumulation. This allowed us to decipher a novel, spatio-temporally regulated  
20 interaction between the JNK-stress response and a genuine tissue-autonomous immune  
21 response. Central to this interaction is the direct inhibition of JNK-signalling by the  
22 antimicrobial peptide Drosomycin, which blocks programmed cell death and prevents  
23 recognition of the stressed tissue by the systemic immune response. While this mechanism  
24 might allow growing salivary glands to cope with temporary stress, continuous expression of  
25 Drosomycin favors survival of unrestricted, hypertrophic *Ras<sup>V12</sup>*-glands. Our findings indicate  
26 the necessity for refined therapeutic approaches that fundamentally acknowledge detrimental  
27 effects that stimulated immune responses have on tissues coping with damage and stress.

28  
29 ***Introduction***

30  
31 Immune and stress responses have evolved to protect the organism from both exogenous and  
32 endogenous stimuli (Eming, 2014; Adamo, 2017; Rankin and Artis, 2018). By sensing  
33 deviations from homeostasis and inducing compensatory mechanisms, immune and stress  
34 responses keep physiological parameters within tolerable limits (Hoffmann and Parsons, 1991;  
35 Vermeulen and Loeschke, 2007).

36 Heat shock, radiation, starvation, toxic metabolites, hypoxia or hyperoxia are all well-  
37 characterized stressors. They activate stress responses which can ultimately lead to the

38 induction of programmed cell death (Lowe et al., 2004; Loboda et al., 2016). In *Drosophila*,  
39 the Keap1-Nrf2-, JNK- and p38-signaling pathways are crucial for mounting these anti-stress-  
40 responses (Stronach and Perrimon, 1999; Fuse and Kobayashi, 2017). Immune responses on  
41 the other hand, like the *Drosophila* Toll and Imd pathways, are typically activated by molecular  
42 structures exposed on the surfaces of pathogens (Medzhitov and Janeway, 2002; Kurata, 2004).  
43 These pathways coordinate the humoral and cellular immune system to eliminate intruding  
44 pathogens (Lemaitre and Hoffmann, 2007; Buchon et al., 2014).

45 Humoral immune responses in *Drosophila* are characterized by the production and  
46 secretion of large sets of effector molecules, most notably antimicrobial peptides (AMPs) like  
47 Drosomycin (Drs) (Imler and Bulet, 2005). AMPs not only target extrinsic threats, but also  
48 react to intrinsic stimuli such as tumorigenic transformation with the possibility to induce  
49 apoptosis (Araki et al., 2018; Parvy et al., 2019). However, it remains unknown whether AMPs  
50 also have functions beyond promoting apoptosis when sensing and reacting to accumulating  
51 stress such as during wound healing and tumor formation.

52 Apart from their described individual roles, immune and stress pathways are proposed  
53 to be either induced successively or concomitantly dependent on the level of deviation from  
54 homeostasis (Chovatiya and Medzhitov, 2014; Ammeux et al., 2016). However, detailed  
55 characterisation of wound healing and tumor models in *Drosophila* revealed a more complex  
56 picture (Park et al., 2004; Buchon et al., 2009; Meyer et al., 2014; Liu et al., 2015; Wu et al.,  
57 2015). Accordingly, immune and stress responses often neither occur separately, nor do they  
58 follow a simple linear cascade, but rather regulate each other via context-dependent mutual  
59 crosstalk (Liu et al., 2015; Liu et al., 2015; Fogarty et al., 2016; Perez et al., 2017). One  
60 recurring motif throughout most of these models is the central role of the stress-responsive  
61 JNK-pathway and its frequent interaction with the Toll and Imd immune pathways (Rämet et  
62 al., 2002; Galko and Krasnow, 2004; Park et al., 2004; Uhlirova et al., 2005; Igaki et al., 2006;  
63 Andersen et al., 2015; Enomoto et al., 2015). However, while JNK-signalling can function  
64 either in a tumor-promoting, anti-apoptotic or in a tumor-suppressive, pro-apoptotic manner  
65 depending on the context, Toll- and Imd-signalling have only been shown to display a tumor-  
66 suppressing, pro-apoptotic role in *Drosophila* (Uhlirova et al., 2005; Igaki et al., 2006; Uhlirova  
67 and Bohmann, 2006; Vidal, 2010; Cordero et al., 2010; Enomoto et al., 2015).

68 These tumor-suppressive, pro-apoptotic functions of immune responses have been well  
69 characterized and attributed to the secretion of humoral factors or the recruitment of immune  
70 cells through the systemic immune system (Babcock et al., 2008; Pastor-Pareja et al., 2008;  
71 Hauling et al., 2014; Parisi et al., 2014; Fogarty et al., 2016; Perez et al., 2017). In addition,

72 during clonal cell competition in imaginal discs, Toll- and Imd-signalling were implicated in  
73 the elimination of less fit cell clones by inducing apoptosis (Meyer et al., 2014). Importantly,  
74 the selective growth disadvantage of these less fit cells is thought to be a response to systemic  
75 infection (Germani et al., 2018) and it remains an open question whether genuine tissue-  
76 autonomous immune responses can contribute to adaptation of growth during wound healing  
77 and tumor formation.

78 The larval salivary gland (SG) of *Drosophila* is a powerful system to study adaptive  
79 growth control, since growth is not completely predetermined, but modulated by the nutritional  
80 status (Smith and Orr-Weaver, 1991; Britton and Edgar, 1998). In contrast to mitotically active  
81 tissues, growth in post-mitotic tissues like the larval SG is based on endoreplication and  
82 hypertrophy rather than on cell division (Edgar et al., 2014; Orr-Weaver, 2015). Modifying the  
83 underlying, tight growth regulation, for instance by continuous growth signalling via  
84 constitutively activated Ras/MAPK-signalling can easily lead to the accumulation of oxidative  
85 stress and DNA damage (Mason et al., 2004; Bartkova et al., 2005; Bartkova et al., 2006; Di  
86 Micco et al., 2006; Shim et al., 2013; Shim, 2015). However, the parameters defining the natural  
87 limit of growth adaptation and the buffering mechanisms in place to cope with prolonged or  
88 continuous stress remain poorly understood.

89 Here, we uncover a genuine tissue-autonomous immune response which directly  
90 regulates hypertrophic growth and adaptation to accumulating stress in larval SGs. By  
91 overexpressing a dominant-active form of the small GTPase Ras, *Ras<sup>V12</sup>*, we induced  
92 hypertrophic growth. This activates a tissue-autonomous immune response which allows the  
93 hypertrophic gland to cope with the resulting stress through spatio-temporally regulated  
94 inhibition of the JNK-mediated stress response. We present evidence that tissue-autonomous  
95 expression of the AMP Drosomycin (Drs) is at the core of this inhibition: Drs directly interferes  
96 with JNK-signalling and inhibits JNK-dependent programmed cell death. This prevents  
97 recognition of the stressed tissue by the systemic immune response and allows survival and  
98 unrestricted growth of hypertrophic salivary glands.

99

## 100 **Results**

101

### 102 ***Local immune reaction accompanies Ras<sup>V12</sup>-dependent hypertrophy***

103 In order to identify buffering mechanisms that compensate for continuous stress, we  
104 made use of our previously published hypertrophy model in the SGs of *Drosophila* larvae  
105 (Hauling et al., 2014). We expressed a dominant-active form of Ras, *Ras<sup>V12</sup>*, uniformly across

106 the entire secretory epithelium of SGs throughout larval development by using the  $Bx^{MS1096}$   
107 enhancer trap (FigS1A for 96/120 h after egg deposition, AED). To further enhance  $Ras^{V12}$ -  
108 dependent hypertrophy, we combined  $Ras^{V12}$ -expression with RNAi-mediated knockdown of  
109 the cell polarity gene *lethal (2) giant larvae* (*lgl*; FigS1;(Jacob et al., 1987; Strand et al., 1994)).  
110 Their individual and cooperative role in tumor formation in mitotic tissues has been well  
111 characterized (Bilder et al., 2000; Pagliarini and Xu, 2003; Herranz et al., 2016). Cell- and  
112 tissue-morphology was assessed using Phalloidin-rhodamine staining (Fig1A/S1A) and nuclear  
113 morphology by DAPI (Fig1B-C/S1B-D).

114 At 96 h AED  $Ras^{V12}$ -expressing SG cells retained most of their normal morphology  
115 compared to  $w^{1118}$ -control glands. However, their integrity and polarity were severely disrupted  
116 at 120 h AED (Fig1A/S1A). Nuclei of  $Ras^{V12}$ -glands showed a continuous increase in volume  
117 at 96 h and 120 h AED (1.33 fold compared to  $w^{1118}$  controls at 96 h AED; 5.66 fold at 120 h  
118 AED; Fig1C) and signs of nuclear disintegration at 120 h AED implying the induction of  
119 programmed cell death (PCD; Fig1B). Both loss of cell integrity and nuclear disintegration  
120 coincided temporarily (Fig1A-B), and were exacerbated upon coexpression of  $lgl^{RNAi}$  (FigS1A-  
121 D). These results confirm our previous findings and demonstrate that continuous growth  
122 signalling in larval salivary glands leads to increased organ size accompanied with additional  
123 endocycles at 96 h AED, both hallmarks of compensatory hypertrophy (Hauling et al., 2014;  
124 Tamori and Deng, 2014). Furthermore, the additional,  $Ras^{V12}$ -induced endoreplications without  
125 obvious effect on tissue integrity imply an adaptability to excess growth signalling, whereas the  
126 subsequent collapse of nuclear integrity and cellular polarity at 120 h AED delineate its  
127 limitations.

128 To characterize the mechanisms involved in the early phase of SG growth adaptation at  
129 96 h AED, we performed total RNA sequencing of complete  $Ras^{V12}$ -expressing and  $w^{1118}$ -  
130 control SGs dissected at 96 h AED prior to cellular and nuclear disintegration. The most  
131 significantly upregulated gene in  $Ras^{V12}$ -glands compared to their  $w^{1118}$ -counterpart was  
132 Ras85D itself (q-value= $6.51 \cdot 10^{-282}$ ), which validates the experimental set-up (Fig1D). The most  
133 differentially expressed gene was the AMP Drs, which indicates the activation of a local  
134 immune response in  $Ras^{V12}$ -glands. To evaluate this further, we employed a GFP reporter for  
135 Drs and observed strong induction in  $Ras^{V12}$ -glands, but not in any other larval tissue  
136 (Fig1E/S1E; Ferrandon et al., 1998a). At 96 h AED the entire secretory epithelium of the SG  
137 expressed Drs with a strong tendency for increased induction in the proximal part (PP) closest  
138 to the duct (Fig1E). At 120 h AED Drs was almost exclusively expressed in the PP (Fig1E/S1E).  
139 In order to assess whether immune cells were recruited as part of a parallel systemic response,



140 we stained glands with an antibody against the pan-hemocyte-marker Hemese. While *Ras<sup>V12</sup>*-  
141 glands were completely devoid of hemocytes at 96 h AED, at 120 h AED they were recruited  
142 to the gland surface. However, hemocyte attachment was restricted to the distal, non-Drs  
143 expressing part (DP), rendering Drs expression and hemocyte attachment across the gland  
144 epithelium mutually exclusive (Fig1E-F). Coexpression of *Ig<sup>RNAi</sup>* elevated the level of recruited  
145 hemocytes at 120 h AED and pre-empted this recruitment to the DP already at 96 h AED  
146 (FigS1E-F).

147 We next investigated whether the change in nuclear volume as a marker for growth  
148 adaptation follows a similar proximal-distal-divide as Drs-expression and hemocyte attachment  
149 (FigS1C). Nuclei in the DP of the SG at 96 h AED showed a moderate volume increase upon  
150 *Ras<sup>V12</sup>*-expression compared to distal *w<sup>1118</sup>*-control nuclei. However, after 120 h AED distal  
151 nuclei had undergone a drastic increase in nuclear volume (6.28 fold compared to distal *w<sup>1118</sup>*-  
152 control nuclei) while nuclei in the proximal part of the SG displayed only a moderate increase  
153 in size compared to *w<sup>1118</sup>*-control nuclei, that did not increase over time. This indicates that  
154 nuclei in the DP of *Ras<sup>V12</sup>*-glands undergo more rounds of endoreplication than their proximal  
155 counterparts coinciding with the decline of Drs-expression and an increase in hemocyte  
156 attachment in this part.

157

### 158 ***Dorsal-dependent Drs expression is part of a genuine tissue-autonomous immune response***

159 As barrier epithelia, the lumen of the SG forms part of a continuum with the exterior,  
160 exposing them to extrinsic stimuli including nutritional cues and pathogens (Andrew et al.,  
161 2000). Since systemic infection can modulate tissue growth, we sought to clarify whether the  
162 observed local immune response in the gland epithelium fulfills the criteria of a genuine tissue-  
163 autonomous immune response or was rather embedded in a wider systemic immune response  
164 (Germani et al., 2018). Therefore, we eradicated any influence by putative systemic infections,  
165 food-derived signals and pathogens or bacterial contamination by raising larvae with *Ras<sup>V12</sup>*-  
166 glands under axenic conditions, on minimal medium or by bleaching embryos (FigS2A'-A''';  
167 Smith and Orr-Weaver, 1991; Britton and Edgar, 1998; Ryu et al., 2008; Piper et al., 2014).  
168 None of these changes diminished the Drs expression, strongly indicating that Drs is indeed  
169 induced in a *bona fide* tissue-autonomous manner as a response to *Ras<sup>V12</sup>*-dependent  
170 hypertrophic growth (FigS2A'-A'''; Colombani et al., 2005; Mirth et al., 2014).

171 We further sought to identify the upstream factors controlling Drs expression. The  
172 homeobox-like transcription factor Caudal is necessary for Drs expression in the female  
173 reproductive organs and the adult SG (Ferrandon et al., 1998a; Han et al., 2004; Ryu et al.,

174 2004). However, RNAi-lines directed against Caudal or its canonical interaction partner,  
175 Drifter/vvl, did not reduce Drs-expression in  $Ras^{V12}$ -glands indicating that the regulation of Drs  
176 expression as part of the tissue-autonomous immune response is clearly different from its  
177 counterpart in the adult SG (FigS2B; Junell et al., 2010).

178 In order to evaluate whether either Toll- or - as is the case for local infections - Imd-  
179 signalling plays a role in Drs expression, we used the reproducible fluorescence pattern of the  
180 Drs-GFP reporter at 96 h AED to assay RNAi-lines directed against canonical components of  
181 both pathways in  $Ras^{V12}$ -glands (Fig2A; see 'Materials and methods' for scored phenotypes;  
182 Ferrandon et al., 1998a; Tzou et al., 2000; Takehana et al., 2004; Wagner et al., 2009). Of the  
183 11 RNAi-lines tested, only one targeting the NF $\kappa$ B-transcription factor Dorsal significantly  
184 reduced the fluorescence signal of the Drs-reporter (Fig2A). However, Drs expression is  
185 completely independent of the upstream modules of the two classical Drosophila immune  
186 pathways, Toll and Imd.

187 At 96 h AED Dorsal was present in the entire secretory epithelium of both  $Ras^{V12}$ - and  
188  $w^{1118}$ -control glands. In contrast, at 120 h AED its expression was confined solely to the PP  
189 (Fig2B). This overlapped with the Drs-mRNA expression as determined by in situ hybridization  
190 (ISH; Fig2SC). Furthermore, both SG-specific knock-down or whole organism homozygous  
191 knock-out ( $dl^{15}$ ) of Dorsal completely abolished Drs-expression in the DP of the gland at 96 h  
192 AED and drastically reduced it in the proximal part at both time points in line with our results  
193 from the reporter assay (Fig2A-B/S2D).

194 Together, our results indicate that the spatio-temporal dynamics of Drs expression are a  
195 consequence of the decrease in endogenous Dorsal expression, independent of canonical Toll-  
196 and Imd-signalling. While regulation of Dorsal expression is  $Ras^{V12}$ -independent, Drs is only  
197 expressed in the presence of Dorsal during  $Ras^{V12}$ -induced hypertrophy (FigS2E).

198

### 199 ***Hypertrophy in SGs induces parallel immune and stress responses***

200 Between 96 h and 120 h AED, the decrease in Drs-expression (Fig1E; Fig2B-C) is  
201 correlated with deterioration of tissue integrity (Fig1A-B) in the DP of hypertrophic  $Ras^{V12}$ -  
202 glands. Thus, we hypothesized that the tissue-autonomous immune response and Drs-  
203 expression aid in preventing the collapse of nuclear as well as cellular integrity until 96 h AED  
204 in the DP and until 120h AED in the PP.

205 To identify possible targets and effector mechanisms of the immune response that buffer  
206 the detrimental effects of hypertrophic growth, we analysed the transcriptome data acquired for  
207 the  $w^{1118}$ -control and  $Ras^{V12}$ -glands at 96 h AED in further detail. In order to distinguish whether

208 the differences between *Ras<sup>V12</sup>*- and *lgl<sup>RNAi</sup>;Ras<sup>V12</sup>*-glands (FigS1B-F) are of quantitative or  
209 qualitative nature and to characterize the PP with its persistent Dorsal and Drs expression in  
210 depth, we also profiled transcriptomes of entire *lgl<sup>RNAi</sup>;Ras<sup>V12</sup>*-glands and solely the proximal  
211 part of *lgl<sup>RNAi</sup>;Ras<sup>V12</sup>*-glands at 96 h AED (FigS3A; see ‘Materials and methods’).

212 The sets of significant and differentially upregulated genes (i.e.,  $\log_2(\text{beta}) \geq 1$ ; *q*-  
213 *value*  $\leq 0.05$ ) for all three conditions (i.e., *Ras<sup>V12</sup>* / *lgl<sup>RNAi</sup>;Ras<sup>V12</sup>* / *lgl<sup>RNAi</sup>;Ras<sup>V12</sup>*-PP each  
214 normalized to *w<sup>1118</sup>*-controls) were intersected to determine common and specific genesets  
215 (Fig3A). Notably, the two biggest genesets are differentially upregulated genes shared between  
216 all three conditions and genes specifically upregulated in the PP (Fig3A). Furthermore, while  
217 all 6 *Ras<sup>V12</sup>*- and *lgl<sup>RNAi</sup>;Ras<sup>V12</sup>*-replicates are in close proximity along the first two principle  
218 components in the PCA, the sets of replicates for *w<sup>1118</sup>* and especially the PP are very distant  
219 from the rest emphasizing the distinctiveness of the PP compared to the rest of the gland (Fig3B).

220 By screening for enriched gene ontology (GO) terms amongst the significantly  
221 upregulated genes in the PP of *lgl<sup>RNAi</sup>;Ras<sup>V12</sup>*-glands in comparison to the entire *w<sup>1118</sup>*-glands,  
222 we identified genes belonging to the GO-term ‘immune response’ (i.e., GO:0006955) as  
223 significantly enriched (Fig3C; *p*-value=1.45·10<sup>-4</sup>). Detailed examination of the fold-enrichment  
224 of these genes across all three experimental groups (i.e., *Ras<sup>V12</sup>* / *lgl<sup>RNAi</sup>;Ras<sup>V12</sup>* / *lgl<sup>RNAi</sup>;Ras<sup>V12</sup>*-  
225 *PP*) showed a preferential expression in the PP, too (17 of 30 genes highest expressed in PP;  
226 blue arrowheads in Fig3C). In addition, 5 of the top 20 upregulated genes in the PP belong to  
227 this GO-term as well. Thus, the Drs-expression we observed using reporter lines serves as a  
228 proxy for a more complex, tissue-autonomous immune response in hypertrophic glands,  
229 especially in the PP. Nonetheless, Drs itself remains one of the top significantly, differentially  
230 upregulated genes across all three conditions (Fig1D; FigS3C; not shown for *lgl<sup>RNAi</sup>;Ras<sup>V12</sup>*). In  
231 fact, Drs-expression in the PP compared to the two conditions for entire glands is even further  
232 increased, confirming the strong tendency for proximal over distal Drs-GFP reporter activation  
233 (Fig1E; Fig2B).

234 A similar GO-term analysis amongst significantly, upregulated genes in entire *Ras<sup>V12</sup>*-  
235 or *lgl<sup>RNAi</sup>;Ras<sup>V12</sup>*-glands revealed the enrichment of genes associated with GO-terms related to  
236 ‘growth’, ‘salivary gland development’ and ‘EGFR signalling’ consistent with the studied  
237 tissue and the induced *Ras<sup>V12</sup>*-overexpression. In addition, the lack of unique, significantly  
238 enriched GO terms and thus distinct gene expression signatures for either *Ras<sup>V12</sup>*- or  
239 *lgl<sup>RNAi</sup>;Ras<sup>V12</sup>*-glands at 96 h AED excludes qualitative differences between these two  
240 genotypes as an explanation for their phenotypic differences (FigS1).

241           Importantly, we detected signatures of an activated JNK-cascade as well as cell death  
242 in *Ras<sup>V12</sup>*- and *Igf<sup>RNAi</sup>;Ras<sup>V12</sup>*-transcriptomes indicating the presence of an activated stress  
243 response and confirming the stimulation of PCD as implied by nuclear disintegration at 120 h  
244 AED (Fig1B;Fig3D/S3B GO:0006955; GO:0008219). To validate these signatures further, we  
245 performed qPCR for canonical JNK-targets at 96 h AED and found that the expression of all  
246 tested genes was significantly increased compared to *w<sup>1118</sup>*-control glands (Fig3E/S3C). We  
247 used the TRE-GFP1b-reporter construct, which recapitulates JNK-activation by expressing  
248 GFP under the control of binding sites for JNK-specific AP-1 transcription factors (Fig3E;  
249 Chatterjee and Bohmann, 2012). This not only confirmed JNK-signalling in *Ras<sup>V12</sup>*-glands, but  
250 also uncovered its prevalence in the DP of these glands at 96 h and 120 h AED consistent with  
251 the transcriptome data (Fig3E/S3C). Moreover, the elevated fluorescence signal in the DP at  
252 120 h AED compared to 96 h AED implies an increase in activation over time correlating with  
253 the collapse of nuclear and cellular integrity during this period (Fig3E/S3C).

254           In summary, the transcriptome analysis confirms our findings that *Ras<sup>V12</sup>*-  
255 overexpression induces a strong tissue-autonomous immune response in the PP of the SG,  
256 beyond sole Drs expression. In contrast, the DP shows a striking increase in JNK-signalling  
257 which correlates with decreasing Drs expression and cellular and nuclear disintegration at 120  
258 h AED, consistent with the described role of JNK target genes in PCD.

259

### 260 ***Drs overexpression and JNK inhibition prevent Ras<sup>V12</sup>-induced tissue disintegration***

261           The increase in JNK-signalling in the DP of the SG as revealed by our transcriptome  
262 analysis coincided in space and time with the downregulation of Drs suggesting an interaction  
263 between the tissue-autonomous immune response and the stress response.

264           To test this assumption, we first overexpressed either Drs or a dominant negative form  
265 of the *Drosophila* Jun kinase basket individually with *Ras<sup>V12</sup>* throughout the entire secretory  
266 epithelium of the SG (Fig4A). Either Drs overexpression or JNK inhibition had a profound  
267 effect on the gland size, which was significantly increased at 120 h AED, compared to *Ras<sup>V12</sup>*  
268 only (Fig4B/S4A).

269           Importantly, despite this size increase, glands of both genotypes (i.e., *Drs,Ras<sup>V12</sup>* /  
270 *bsk<sup>DN</sup>;Ras<sup>V12</sup>*) showed no morphological abnormalities and resembled control *w<sup>1118</sup>*- much  
271 more than *Ras<sup>V12</sup>*-glands (Fig4A-B). Strikingly, *bsk<sup>DN</sup>;Ras<sup>V12</sup>*- and *Drs,Ras<sup>V12</sup>*-glands were  
272 completely devoid of attached hemocytes (Fig4B-C). Given the basement membrane's (BM)  
273 role in directly regulating organ morphology, the rescue of the gland shape upon coexpression  
274 of either Drs or *bsk<sup>DN</sup>* with *Ras<sup>V12</sup>* pointed towards changes in the integrity of the BM (Ramos-

275 Lewis and Page-McCaw, 2019). In addition, previous reports suggested that hemocytes are only  
276 recruited to tissue surfaces upon tissue disintegration and when the integrity of the BM is lost  
277 (Kim and Choe, 2014). Hence, to trace the BM we used an endogenous GFP-trap in the *viking*  
278 gene, which encodes one subunit of CollagenIV (Fig4B-C). Both in the presence of Drs or by  
279 inhibiting basket, the BM remained a continuous sheet surrounding the entire gland, whereas  
280 the BM on the surface of *Ras<sup>V12</sup>*-glands was clearly disrupted.

281 Matrix metalloproteinases (MMPs) are likely candidates for executing the disruption of  
282 the BM and known target genes of the JNK-pathway (Hauling et al., 2014; Stevens and Page-  
283 McCaw, 2012; Uhlirova and Bohmann, 2006). In order to see whether hypertrophic glands  
284 express MMPs, we performed qPCR for MMP1 and MMP2 at 96 h and 120 h AED on *Ras<sup>V12</sup>*-  
285 and control *w<sup>1118</sup>*-glands. At 96 h AED, *Ras<sup>V12</sup>*-glands already exhibit increased MMP1  
286 expression (Fig4C-D). However, MMP2 only reaches a significant level of expression at 120 h  
287 AED coinciding with the appearance of hemocyte attachment (Fig4D). SG-wide, *Ras<sup>V12</sup>*-  
288 independent overexpression of MMP2, but not of MMP1, caused opening of the BM and  
289 hemocyte attachment to the surface (Jia et al., 2014). This indicates the necessity for a JNK-  
290 dependent expression of MMP2 in the hypertrophic *Ras<sup>V12</sup>*-glands prior to the recruitment of  
291 hemocytes to the tissue surface (Fig4E/S4B).

292 Taken together, overexpression of Drs alone is sufficient to mimic the inhibition of the  
293 JNK-pathway in *Ras<sup>V12</sup>*-glands: both lead to excess hypertrophic growth compared to *Ras<sup>V12</sup>*-  
294 glands, but simultaneously prevent tissue disintegration and PCD. Prohibiting the disruption of  
295 the basal membrane inhibits hemocyte recruitment and thus prevents the systemic immune  
296 response from sensing hypertrophic growth. This in turn suggests that the endogenous Drs  
297 expression in *Ras<sup>V12</sup>*-glands is seminal for maintaining nuclear and tissue integrity and thus part  
298 of the buffer mechanism to adapt to continuous growth signalling.

299

### 300 ***Drs inhibits JNK-signalling***

301 The strong correlation between loss of Drs and the increase in JNK-signalling in the DP  
302 of *Ras<sup>V12</sup>*-glands between 96 h and 120 h AED indicated an active interaction between Drs and  
303 the JNK-pathway, which prompted us to resolve their hierarchy by epistatic analysis.

304 Coexpression of *bsk<sup>DN</sup>* with *Ras<sup>V12</sup>* did not deplete Drs in the proximal part of 120 h-old  
305 glands, since neither the fluorescence signal of the Drs-GFP reporter nor staining for  
306 endogenous *Drs*-mRNA via ISH showed any effects, which excludes a direct regulation of Drs  
307 by JNK-signalling (Fig4A;FigS5A). qPCR for Drs in *Ras<sup>V12</sup>*- and *bsk<sup>DN</sup>;Ras<sup>V12</sup>*-glands  
308 confirmed these results further (FigS5B). In contrast, qPCR in hypertrophic *Ras<sup>V12</sup>*-glands



309 showed a significant reduction in expression of JNK target genes upon coexpression of Drs at  
310 96 h and 120 h AED (Fig5B/S5C-D), in line with a decrease in activated basket (Fig5C,E) and  
311 TRE-GFP1b signal in *Drs,Ras<sup>V12</sup>*- compared to *Ras<sup>V12</sup>*-glands (Fig5B,D,F). Thus, the  
312 overexpression of the AMP Drs actively and tissue-autonomously inhibits the JNK-dependent  
313 stress response in hypertrophic *Ras<sup>V12</sup>*-glands beyond 96 h AED.

314 In addition, we used an efficient RNAi-line against Drs, which in combination with  
315 *Ras<sup>V12</sup>* reduced Drs-expression drastically compared to its expression in *Ras<sup>V12</sup>*-glands  
316 (FigS5C-D). All significantly upregulated JNK-target genes in *Ras<sup>V12</sup>*-glands apart from *upd2*  
317 were further increased upon knockdown of Drs at 96 h AED (FigS5C). However, this effect  
318 ceased at 120 h AED consistent with the canonical loss of Drs expression in the DP of *Ras<sup>V12</sup>*-  
319 glands (Fig5D). This result demonstrates that until 96 h AED the endogenously expressed Drs  
320 has the same inhibitory effect on the JNK-pathway as the Drs-overexpression has at 120 h AED.

321

### 322 ***Drs prevents cell death in Ras<sup>V12</sup>-glands***

323 The capacity to induce apoptosis is a well-established function of the JNK-pathway in  
324 *Drosophila* (Uhlirva et al., 2005; Igaki et al., 2006; Uhlirva and Bohmann, 2006; Cordero et  
325 al., 2010; Enomoto et al., 2015). Combined with the identification of ‘cell death’ as a  
326 significantly enriched term in the GO-analysis, we hypothesized that the observed nuclear  
327 disintegration in *Ras<sup>V12</sup>*-glands after 96 h AED was a consequence of the JNK-dependent  
328 induction of PCD (Fig1B-C/S1B-D; Fig3D/S3B).

329 In mitotic tissues, the apoptotic inducer *head involution defective* (*hid*) is inhibited by  
330 Ras/MAPK-signalling (Bergmann et al., 1998; Kurada and White, 1998). However, in *Ras<sup>V12</sup>*-  
331 glands *hid* expression gradually increased from 96 h to 120 h AED coinciding with the increase  
332 in nuclear disintegration (Fig6A). Coexpression of Drs with *Ras<sup>V12</sup>* significantly decreased *hid*  
333 expression at both time points, while Drs knock-down in *Ras<sup>V12</sup>*-glands increased *hid*  
334 expression even further already at 96 h AED. Together with the reduction in *hid* expression  
335 upon JNK-inhibition in *bsk<sup>DN</sup>;Ras<sup>V12</sup>*-glands, Drs emerges as a negative regulator of the  
336 apoptotic inducer *hid* by inhibiting JNK-signalling (FigS5B).

337 To evaluate the induction of PCD in *Ras<sup>V12</sup>*-glands, we either inhibited JNK-signalling  
338 at the level of basket activation or coexpressed the caspase-inhibitor p35 with *Ras<sup>V12</sup>* and  
339 examined nuclear volume and integrity (Fig6B-D). p35 inhibits Drice and thus blocks PCD at  
340 the level of effector caspase activation (Hawkins et al., 2000; Hay et al., 1994; Meier et al.,  
341 2000). While both interventions successfully blocked nuclear disintegration, the additional  
342 rounds of endoreplication as observed in *Ras<sup>V12</sup>*-glands were not suppressed (Fig6C-D).



343 Crucially, Drs-coexpression in *Ras<sup>V12</sup>*-glands phenocopies the inhibition of JNK-signalling and  
344 effector caspases both in terms of restoring nuclear integrity as well as the persistence of excess  
345 endoreplications.

346 Last, to validate the inhibition of PCD by Drs, we monitored Dronc activity using the  
347 cleaved caspase 3 antibody (CC3). In fact, the strongest Dronc activity occurred in cells that  
348 also displayed heavy disintegration of nuclei, confirming the relation between caspase  
349 activation and nuclear disintegration as part of PCD (FigS6A-B). However, in *Drs,Ras<sup>V12</sup>*-  
350 glands Dronc was significantly less activated compared to *Ras<sup>V12</sup>*-glands (Fig6E-F; Fan and  
351 Bergmann, 2010).

352 Taken together, we show that JNK-dependent induction of PCD is a consequence of the  
353 collapse in adaptation to *Ras<sup>V12</sup>*-induced hypertrophy. Importantly, overexpression of Drs in  
354 *Ras<sup>V12</sup>*-glands prevents PCD by blocking full JNK-activation. This is in contrast to recent  
355 observations where AMPs, including Drs, act pro-apoptically aiding in the elimination of tumor  
356 cells and limiting tumor size (Araki et al., 2018; Parvy et al., 2019).

357

### 358 ***Drs inhibits the JNK-feedback loop***

359 Various *Drosophila* models for tissue transformation have shed light on the functional  
360 separation of the JNK-pathway into an upstream kinase cascade leading to basket-activation  
361 and a downstream feedback-loop converging again on basket activation (Fig7A; Shlevkov and  
362 Morata, 2012; Fogarty et al., 2016; Muzzopappa et al., 2017; Perez et al., 2017).

363 Our results revealed a negative regulatory impact of Drs on JNK-signaling in *Ras<sup>V12</sup>*-  
364 glands, but did not determine which part of the pathway is targeted by Drs. To answer this  
365 question, we uncoupled the feedback loop from the upstream kinase cascade by solely  
366 overexpressing *hid* (Fig7A). Irrespective of the differing models for the signal propagation  
367 downstream of Dronc, this initiator caspase remains seminal for establishing the actual  
368 feedback with basket (Shlevkov and Morata, 2012; Fogarty et al., 2016). Thus, we stained  
369 glands for activated Dronc and basket after a pulse of *hid*-overexpression during the larval  
370 wandering stage (Fig7A). As expected, *hid*-expressing glands showed highly elevated levels of  
371 activated Dronc, but also basket, which indicates the presence of feedback activation. Moreover,  
372 both phenotypes were reversed upon coexpression of Drs during the *hid*-expression pulse  
373 (Fig7B-C,E). Thus, Drs seems to inhibit JNK-signalling downstream of *hid* and upstream of  
374 Dronc and basket, emphasizing an inhibition of the JNK-feedback loop rather than the initial  
375 kinase cascade.

376 To clarify that Drs operates in a similar fashion during *Ras*<sup>V12</sup>-induced hypertrophic  
377 growth, we stained *Ras*<sup>V12</sup>-glands (Fig6E-F) for activated basket in the presence and upon  
378 knock-down of Dronc (Fig7D,F/S7A-B). In fact, the absence of a signal for activated basket in  
379 *Dronc*<sup>RNAi</sup>;*Ras*<sup>V12</sup>- compared to strong *Ras*<sup>V12</sup>-glands confirms the presence of a genuine  
380 feedback-regulation as part of JNK-signalling in SGs.

381

## 382 ***Discussion***

383

### 384 ***Tissue-autonomous vs. systemic immune response mediated via JNK-signalling***

385 By overexpressing *Ras*<sup>V12</sup> in larval SGs, we made use of and overrode the gland's ability  
386 to adapt to growth signals. Activating constitutive Ras/MAPK-signalling allowed us to identify  
387 local immune and stress responses as part of a buffering mechanisms to compensate the  
388 accumulation of stress and decipher natural limits of growth adaptation (Hauling et al., 2014).  
389 Remarkably, in this context the local immune response inhibits the parallel stress response, an  
390 effect that to our knowledge has not been described before. Central to this inhibition is the AMP  
391 Drs, which directly impinges on the JNK-pathway and thereby subsequently also on inducing  
392 apoptosis, a function completely opposite to previous observations in other tissues (Araki et al.,  
393 2018; Parvy et al., 2019). These results also indicate an unprecedented role for an AMP as a  
394 signal transducer enabling tissue-autonomous crosstalk between immune and stress pathways.  
395 Dependent on the extent of JNK-inhibition by the local, Drs-dependent immune response and  
396 thus the integrated decision of both on the state of the tissue's homeostasis, the gland epithelium  
397 attracts hemocytes as part of a wider, systemic immune response. By virtue of inhibiting JNK-  
398 signalling, tissue-autonomous and systemic immune response antagonize each other, a balance  
399 that decides on continuous hypertrophic growth or its restriction (Fig8). The latter has far  
400 reaching implications for therapeutic approaches that need to consider the adverse effects that  
401 stimulating immune responses might have on tissue growth after damage and under stress.

402

### 403 ***Drs is expressed as part of a genuine tissue-autonomous immune response***

404 The salivary glands of *Drosophila* larvae are an integral part of its gastrointestinal  
405 system and the lumen of the mature glands forms a continuum with the exterior. As such the  
406 glands are constantly exposed to microbial and pathogenic influences, which predestines them  
407 to be a dedicated immunological barrier epithelium. However, raising larvae with *Ras*<sup>V12</sup>-glands  
408 under strictly axenic conditions corroborated the authenticity of the immune response as truly  
409 tissue-autonomous and thus independent of exogenous or systemically distributed pathogenic

410 stimuli. This is further emphasized by the dependency of Drs expression on the tissue-specific  
411 overexpression on *Ras*<sup>V12</sup> and tissue-autonomous manipulations (i.e., Drs or bsk<sup>DN</sup>  
412 overexpression) leading to the inhibition of JNK-activation and hemocyte recruitment.

413 However, apart from Dorsal neither the homeobox transcription factor Caudal as in the  
414 adult glands nor any other of the canonical members belonging to the Toll- and Imd-pathway  
415 are involved in Drs expression (Ferrandon et al., 1998b; Hauling et al., 2014; Ryu et al., 2004).  
416 Under wild-type conditions, Dorsal is expressed throughout the entire gland epithelium until  
417 96 h AED, but only remains expressed in the PP at 120 h AED (Fig2B). This spatio-temporal  
418 expression pattern in turn determines the expression of Drs in *Ras*<sup>V12</sup>-glands essentially  
419 separating the gland at 120 h AED into an immunocompetent duct-proximal and a stress-  
420 responsive duct-distal compartment (Fig2B, Fig8). Due to the absence of Drs in the DP at 120  
421 h AED, stress-responsive JNK-signalling finally exceeds a critical threshold leading to elevated  
422 MMP2- and hid-expression. This stimulates the onset of PCD and opening of the basal  
423 membrane as a prerequisite for attachment of hemocytes that are subsequently recruited to the  
424 surface of the SGs (FigS2E, Fig8; Hauling et al., 2014). To the contrary, Dorsal continues to  
425 induce Drs in the PP of *Ras*<sup>V12</sup>-glands until 120 h AED in line with the complete absence of  
426 hemocyte recruitment to this part of the gland (Fig1F/S1B-C).

427

### 428 ***Drosomycin impinges on JNK feed-back activation***

429 In depth analysis of wound regeneration and tumor formation has shed light on the  
430 intricate architecture of the JNK-pathway and its signal propagation (Santabarbara-Ruiz et al.,  
431 2015; Pinal et al., 2018). This has led to the discovery of feedback- or self-sustenance-loops as  
432 part of JNK-signalling (Shlevkov and Morata, 2012; Fogarty et al., 2016; Muzzopappa et al.,  
433 2017; Perez et al., 2017). Similarly, several lines of evidence validated the existence of a  
434 complex quantitatively and qualitatively regulated activation of the JNK-pathway in *Ras*<sup>V12</sup>-  
435 glands. In fact, the strong reduction of basket activation upon knock-down of the initiator  
436 caspase Dronc in the *Ras*<sup>V12</sup>-background at 120 h AED indicates that a feedforward-loop is also  
437 part of the propagation of JNK-activation in hypertrophic glands (Fig7D,F/S7A-B).  
438 Consistently, even sole hid overexpression in SGs led to Dronc as well as basket activation  
439 emphasizing the presence of this feedback-regulation as part of the JNK-pathway further  
440 (Fig7B-C,E).

441 In general, feedback loops serve as a predestined platform to integrate additional signals  
442 via crosstalk with other pathways to dynamically modulate the originally, transmitted signal  
443 and thus either amplify or weaken the response (Antebi et al., 2017; Kholodenko, 2006). Here,

444 we describe a novel mode of signal attenuation by the tissue-autonomous immune response that  
445 rather than eliminating an exogenous stimulus directly interferes with the signal propagation in  
446 the JNK-feedback loop. Fundamentally, this interaction is part of an emerging picture of  
447 crosstalk between immune and stress responses involved in organ growth and maintenance in  
448 *Drosophila* (Hauling et al., 2014; Liu et al., 2015; Parisi et al., 2014; Wu et al., 2015).

449 Drs regulates the signal propagation of the intracellular module of the JNK-pathway  
450 and throughout our experiments only directly Drs expressing cells prevented *Ras<sup>V12</sup>*-induced  
451 cell disintegration and PCD. However, it remains an outstanding question whether Drs  
452 functions exclusively cell-autonomously and intracellularly or whether secreted Drs operates  
453 in an autocrine manner too. Clonal analysis and rescue experiments will serve this purpose in  
454 the future. Further work on the effector mechanism of Drs will also elucidate further details  
455 about the components of the JNK-feedback loop in- or directly regulated by Drs. This will also  
456 contribute to mapping the manifold modes of immune-stress-crosstalk in *Drosophila* and find  
457 general patterns among them beyond a sole dependency on the specific context.

458

#### 459 ***Drs promotes hypertrophic growth and inhibits PCD***

460 As our *Drs, Ras<sup>V12</sup>*-experiments indicated, under conditions of continuous growth and  
461 therefore chronic stress induction, the ability to suppress the JNK-pathway in a Drs-dependent  
462 manner supports continuous, hypertrophic growth of *Ras<sup>V12</sup>*-glands and the survival of the  
463 tissue. Moreover, a prolongation of Drs-expression beyond its endogenous decrease inhibits the  
464 induction of PCD and the recognition of the systemic immune response and thus renders the  
465 hypertrophic gland unchallenged.

466 In fact, while Ras/MAPK-signalling in mitotic tissues crucially suppresses apoptosis by  
467 downregulating hid expression, this effect is revoked in hypertrophic *Ras<sup>V12</sup>*-glands (Bergmann  
468 et al., 1998; Kurada and White, 1998). While the reason for this difference remains to be  
469 elucidated, it is in fact Drs which operates as the inhibitor of apoptotic inducers in hypertrophic  
470 glands. This function is central to the suppression of PCD in *Ras<sup>V12</sup>*-glands (Fig6A).

471 This differs fundamentally from the pro-apoptotic function of AMPs, which was recently  
472 described for two tumor models. In both disc (discs large, *dlg*, Parvy et al., 2019) and leukemic  
473 tumors (*mxc<sup>mbn1</sup>*, Araki et al., 2018), AMPs were shown to target tumor cells and limit tumor  
474 size by inducing apoptosis. In addition to the differences between the tumorous tissues (i.e.,  
475 proliferative discs and lymph glands), the fact that Drs is induced locally in SGs and acts tissue-  
476 autonomously may explain its different activities.

477

## 478 ***Hypertrophic SGs are a remarkable system to discover buffer mechanisms***

479 Being incapable of cell proliferation, damaged postmitotic tissues can't rely on  
480 regenerative cell plasticity like imaginal discs or stem cell-derived tissue regeneration as in the  
481 *Drosophila* adult midgut (Ohlstein and Spradling, 2006; Herrera et al., 2013; Herrera and  
482 Morata, 2014; Schuster and Smith-Bolton, 2015; Ahmed-de-Prado and Baonza, 2018). Instead,  
483 they need to cope with endogenous and exogenous influences via elaborate mechanisms to  
484 prevent or buffer detrimental consequences.

485 Here, we show that continued *Ras*<sup>V12</sup>-expression in the larval salivary gland overrides  
486 the dependency on nutritional cues and stimulates excess endoreplications that eventually have  
487 damaging effect on the tissue integrity by inducing elevated levels of stress. Uninterrupted  
488 induction of endoreplications has its natural limits in every system, even in salivary glands that  
489 are already polyploid. Eventually, continuous induction of more endocycles is challenged by  
490 nutritional restrictions in synthesizing more DNA, replication stress, spatial limitations in the  
491 gland nuclei and continuously more unsynchronized metabolic turnover. Hence, in spite of the  
492 anti-apoptotic function *Ras*<sup>V12</sup> conveys in mitotic tissues, unrestricted stimulation of excess  
493 endoreplications ultimately leads to cell death. Since this characterizes the final collapse of  
494 tissue homeostasis, it also allows to study the extent of buffering capacity conveyed by immune  
495 and stress-responsive signalling.

496 Thus, hypertrophic *Ras*<sup>V12</sup>-glands constitute an outstanding system to study the  
497 involvement of tissue-autonomous immune and stress-induced responses to buffer deviation  
498 from homeostasis.

499

## 500 ***Immune surveillance theory***

501 According to the immune surveillance theory, the immune system has evolved to reduce  
502 the risk of somatic cells accumulating cancerous mutations (Burnet, 1970; Burnet, 1957). In  
503 order to reduce the danger of cell-transformation, cells express or expose molecules upon  
504 recognition of stress or damage during transformation. These markers are sensed by the immune  
505 system, which in turn eradicates the potentially harmful cells. (Jung et al., 2012; Vantourout et  
506 al., 2014; Schmiedel and Mandelboim, 2018). However, the immune surveillance theory  
507 remains controversial, since tumor-associated inflammation was also shown to promote rather  
508 than suppress tumor growth (Balkwill and Mantovani, 2001; Mantovani et al., 2008). Our  
509 model bridges the gap between these two opposing views, since the effects of the tissue-  
510 autonomous and systemic immune responses appear to be antagonistic regarding the regulation  
511 of JNK-activation and thus ultimately PCD. In fact, only the integration of the various stress

512 and immune mechanisms in hypertrophic *Ras*<sup>V12</sup>-glands allows a concerted decision to  
513 eradicate a putatively dangerous cell via inducing PCD or not. Given the evolutionary  
514 conservation from insects to mammals of signalling pathways that govern growth control  
515 (Edgar, 2006), it is likely that mechanisms to detect and counteract a loss in regulation of these  
516 pathways, such as stress and immune pathways, are similarly conserved between both phyla.  
517

## 518 ***Material and methods***

519

### 520 ***Fly husbandry and stocks***

521 All crosses were reared on standard potatomash/molasses medium under tempered conditions (see  
522 'Staging') in a 12h dark/12 h light-cycle. Drs-GFP (W.-J. Lee), UAS-dfr<sup>RNAi</sup> (S.Certel), TRE-GFP1b (D. Bohmann),  
523 UAS-Drs (B. Lemaitre), dl<sup>15</sup> (Y. Engström), UAS-hid (M.Suzanne), UAS-MMP2<sup>#4</sup>, UAS-MMP1<sup>APM1037</sup> and UAS-  
524 MMP1<sup>APM3099</sup> (A. Page-McCaw) were kind gifts from the indicated donors. The generation of the CollagenIV  
525 flytrap line vkg<sup>G00454</sup> was described in (Morin et al., 2001). Please, see supplementary file 1 for complete list of  
526 experimental crosses.

527

### 528 ***Staging***

529 Virgins were collected for 3-7 d before setting crosses. Initially, crosses were kept on standard food  
530 without antibiotics for 48 h at 25°C. Eggs were collected for 6 h (Immunohistochemistry and qPCR) or for 2 h  
531 (RNASeq) at 25°C. When necessary, precollections were performed for 2 h at 25°C prior to the actual collection.  
532 Egg collections were incubated for 24 h at 29°C or for hid experiments 48 h at 18°C and batches of 24 hatched 1<sup>st</sup>  
533 instar larvae were afterwards transferred to vials with 3 ml standard food supplemented with Neomycin (0.1  
534 mg·ml<sup>-1</sup>, Sigma-Aldrich, N1876), Vancomycin (0.1 mg·ml<sup>-1</sup>, Sigma-Aldrich, V2002), Metronidazol (0.1 mg·ml<sup>-1</sup>,  
535 Sigma-Aldrich, M3761) and Carbenicillin (0.1 mg·ml<sup>-1</sup>, Sigma-Aldrich, C1389). After incubation at 29°C for  
536 another 72 h (96 h AED) or 96 h (120 h AED), 3<sup>rd</sup> instar larvae were prepared for dissection or pictures were taken  
537 of whole larvae with a Leica MZ FLIII Fluorescence Stereomicroscope. For hid experiments, transferred larvae  
538 were incubated for 197 h at 18°C, shifted to 29°C for 12 h and finally dissected. To exclude microbial  
539 contamination and maintain germ-free conditions, BxGal4;;DrsGFP/UAS-Ras<sup>V12</sup>-eggs were dechorionated with a  
540 50% Sodium Hypochlorite solution (Fisher Scientific, 10401841) immediately after collection and transferred to  
541 vials with apple-agar supplemented with Nipagin, Propionic acid and the same antibiotics as above. Larvae were  
542 then analysed at 24 h and 48 h AED.

543

### 544 ***Drs reporter assay***

545 Replicates of *Drosophila* larvae (n=24 larvae·replicate<sup>-1</sup>; N>6 replicates) at 96 h AED were screened for  
546 Drs-GFP reporter signals. Three phenotypes were distinguished: (1.) "Full" SG pattern includes GFP signal across  
547 the entire PP and GFP<sup>+</sup>-cells with reduced intensity in the DP. (2.) "Partial" SG is GFP<sup>+</sup> throughout the PP, but  
548 less pronounced in DP with reduced signal intensity and fewer GFP<sup>+</sup>-cells. (3.) "None" phenotype lacks signal  
549 throughout the entire gland. Distribution of phenotypes were scored per replicate and significance calculated for  
550 the "None"-phenotype via Dunn's test after performing the Kruskal-Wallis rank sum test.



551

## 552 **qPCR**

553 Total RNA of dissected salivary glands was isolated with the RNAqueous-Micro Kit (ThermoFisher  
554 Scientific, AM1931) and from whole larvae with the RNAqueous Kit (ThermoFisher Scientific, AM1912)  
555 according to the instructors manual. Residual genomic DNA was digested with RNase-free DNaseI (ThermoFisher  
556 Scientific, EN0521) and cDNA reverse transcribed with SuperscriptIII (ThermoFisher Scientific, 18080-093)  
557 while using oligo(dT)<sub>16</sub>-primer (ThermoFisher Scientific, 8080128). Quality of all prepared totalRNA-extractions  
558 was evaluated on a 5 mM Guanidinium Thiocyanate-agarose gel, for optimization purposes on a BioRad Experion  
559 system (RNA StdSens Assay, 7007153, 7007154) and totalRNA for sequencing was run on a 2100 Bioanalyzer  
560 Instrument (Agilent Technologies, 5067-1511). qPCR reactions were set as technical triplicates with KAPA SYBR  
561 FAST qPCR Master Mix (KR0389, v9.13) including 200 nM final concentration of forward and reverse primers  
562 and run on a Rotor-Gene Q 2plex HRM machine (9001550). See supplementary file 2 for list of all used qPCR  
563 primers.

564

## 565 ***RNASeq library preparation and analysis***

566 To avoid variability and thus confounding influences among the various RNASeq sample groups, we  
567 controlled rigorously for age of female parents, larval density to avoid larval crowding, age differences as well as  
568 developmental age itself and bacterial influences by using axenic culture conditions.

569 Poly(A)-containing mRNA molecules from totalRNA-samples were purified with oligo(dT)-magnetic  
570 beads, subsequently fragmented and cDNA synthesised with random primers using the TruSeq RNA Sample  
571 Preparation Kit v2. Adapter ligation and PCR-amplification precede cluster formation with a cBot cluster  
572 generation system. All samples were sequenced on a HiSeq 2500 Illumina Genome Sequencer as PE50. Reads  
573 were pseudoaligned with kallisto (v0.44.0) to a transcriptome index derived from all *Drosophila* transcript  
574 sequences of the dmel release r6.19. Subsequent analysis of transcript abundances was performed in R with sleuth  
575 (v0.30.0) including principal component analysis for dimensionality reduction, statistical and differential  
576 expression analysis based on the beta statistic derived from the wald test. Enriched gene ontology terms were  
577 identified by calculating hypergeometric p-values via the GOstats (v2.48.0) R package. Gene IDs were converted  
578 via the AnnotationDbi (v1.44.0) package and the reference provided with the org.Dm.eg.db (v3.7.0) database and  
579 geneset intersections visualized as UpSetR plot (v1.3.3). Please, see the accompanied R markdown deposited on  
580 GitHub for details ([https://github.com/robertkrautz/sg\\_analysis](https://github.com/robertkrautz/sg_analysis)).

581

## 582 ***Immunohistochemistry***

583 Proximal parts of staged larvae were inverted in PBS, unnecessary organs removed and samples fixed in  
584 4% paraformaldehyde for 20 min. Subsequently, samples were washed three times for each 10 min in PBS or  
585 PBST (1% TritonX-100). Blocking was performed with 0.1% BSA in PBS (H2) or 5% BSA in PBST (anti-CC3,  
586 anti-pJNK and anti-Dorsal). Samples were then incubated in primary antibodies dissolved in blocking buffer for  
587 12 h at 4°C or 1 h at room temperature (RT). Primary antibodies comprised rabbit anti-cleaved caspase 3 (1:200,  
588 Cell Signalling Technology, 9661), mouse anti-pJNK (1:250, Cell Signalling Technology, 9255), mouse anti-  
589 Dorsal (1:50, DSHB, 7A4) and mouse anti-Hemese (1:5; gift from István Andó). After washing as prior to blocking,  
590 secondary antibodies were applied together with DAPI (1:500; Sigma-Aldrich; D9542) and when necessary

591 Phalloidin-546 (1:500, Molecular probes, A22283) in blocking buffer for 1 h at RT. As secondary antibodies goat  
592 anti-Mouse-IgG-Alexa546 (H+L; 1:500; ThermoFisher Scientific; A-11030) and goat anti-Rabbit-IgG-Alexa568  
593 (H+L; 1:500; ThermoFisher Scientific; A-11011) were employed. Final washing as prior to blocking preceded  
594 dissection of the samples in PBS and separation of salivary glands. Tissues were mounted in Fluoromount-G  
595 (SouthernBiotech) and analysed with a Zeiss LSM780 confocal microscope. Images were extracted with Zen  
596 software (Blue edition) for further processing either in Adobe Photoshop CS5 Extended (v12.0.4 x64) or Inkscape  
597 (v0.92).

598

### 599 ***Hemocyte- / pJNK- / CC3- quantification and size measurement***

600 Pictures of stained glands were taken with a Zeiss Axioplan 2 microscope equipped with an  
601 ACHROPLAN 4x lens and a Hamamatsu ORCA-ER camera (C4742-95). Images were extracted with AxioVision  
602 software (v40V 4.8.2.0) and analysed with ImageJ. Cumulated area of hemocyte attachment, pJNK or CC3  
603 fluorescence per SG or per SG part was filtered in the Red-channel and gland size determined by outlining glands,  
604 PPs or DPs with the 'Polygon selection'-tool. The distribution of hemocytes in *Drosophila* can be approximated  
605 by a natural logarithm, which required transformation of hemocyte attachment- and SG-areas before calculating  
606 ratios (Sorrentino, 2010). Normality across all samples of a particular genotype and where necessary separated by  
607 gland part (i.e., proximal or distal) or time (i.e., 96 h and 120 h AED) was evaluated with the Shapiro-Wilk-test  
608 and by bootstrapping via the fitdistrplus R package (v1.0.11). Significant differences between experimental groups  
609 were determined for pairwise comparisons via the Student's t-test after validating un-/equal variance via the  
610 Bartlett's test. Data and statistical analysis was performed in R.

611

### 612 ***Nuclei volume***

613 Z-stacks of entire salivary glands were captured with a Zeiss LSM780 confocal microscope for DAPI  
614 signal. Obtained stacks were further processed in ImageJ via the '3D Object Counter' plugin. Proximal and distal  
615 compartments were defined with the 'Polygon selection'-tool. Transfer of the region of interest to all z-stack slices,  
616 signal thresholding, object identification and volume determination were integrated in a macro workflow. Data  
617 were plotted as average nucleus volume for all nuclei of individual glands or gland parts. Representative sections  
618 of individual z-stack slices showing the transition between proximal and distal compartments were cropped and  
619 added for illustration. Statistics were performed similar to the analysis of Hemocyte-, pJNK- and CC3-  
620 quantifications.

621

### 622 ***In situ hybridization***

623 Proximal parts of staged larvae were separated from the larval body in PBS, transferred to fixative (4%  
624 PFA), washed 4 times for 15 min in PBS and stored at -20°C in methanol. A cDNA for the Drs locus (LP03851)  
625 was obtained from DGRC. Probe synthesis and detailed ISH procedure is described elsewhere (Hauptmann, 2015).  
626 Stained salivary glands were mounted in Fluoromount-G (SouthernBiotech) and images were captured with a  
627 Leica MZ16 microscope combined with a Leica DFC300Fx camera.

628

### 629 ***Acknowledgements***

630

631 We would like to thank S. Höglund and the Imaging facility at Stockholm University for  
632 microscopy support, the Bloomington Drosophila Stock Center and the Vienna Drosophila  
633 Resource Center for fly stocks, the Drosophila Genomics Resource Center for the Drs cDNA,  
634 the Developmental Studies Hybridoma Bank for the anti-Dorsal antibody and D. Bohmann,  
635 S.Certel, Y. Engström, W.-J. Lee, B. Lemaitre as well as M. Suzanne for providing us with flies.  
636 We are especially grateful to R. Karlsson, I. Söll and G. Hauptmann for decisive feedback on  
637 experimental procedures and J. van den Aemele for his critical review of the manuscript. This  
638 work was supported by the Swedish Research Council (VR-2010-5988 and VR 2016-04077)  
639 and the Swedish Cancer Foundation (CAN 2010/553 and CAN 2013/546).

640

## 641 *References*

642

643 Adamo, S.A. (2017). Stress responses sculpt the insect immune system, optimizing defense in  
644 an ever-changing world. *Dev Comp Immunol* 66, 24-32.

645 Ahmed-de-Prado, S., and Baonza, A. (2018). Drosophila as a Model System to Study Cell  
646 Signaling in Organ Regeneration. *Biomed Res Int* 2018, 7359267.

647 Ammeux, N., Housden, B.E., Georgiadis, A., Hu, Y., and Perrimon, N. (2016). Mapping  
648 signaling pathway cross-talk in Drosophila cells. *Proc Natl Acad Sci U S A* 113, 9940-9945.

649 Andersen, D.S., Colombani, J., Palmerini, V., Chakrabandhu, K., Boone, E., Rothlisberger,  
650 M., Toggweiler, J., Basler, K., Mapelli, M., Hueber, A.O., *et al.* (2015). The Drosophila TNF  
651 receptor Grindelwald couples loss of cell polarity and neoplastic growth. *Nature* 522, 482-  
652 486.

653 Andrew, D.J., Henderson, K.D., and Seshaiiah, P. (2000). Salivary gland development in  
654 Drosophila melanogaster. *Mech Dev* 92, 5-17.

655 Antebi, Y.E., Nandagopal, N., and Elowitz, M.B. (2017). An operational view of intercellular  
656 signaling pathways. *Curr Opin Syst Biol* 1, 16-24.

657 Araki, M., Awane, R., Sato, T., Ohkawa, Y., and Inoue, Y. (2018). Anti-tumor effects of  
658 antimicrobial peptides, targets of the innate immune system, against hematopoietic tumors in  
659 Drosophila mxc mutants. *BioRxiv*.

660 Babcock, D.T., Brock, A.R., Fish, G.S., Wang, Y., Perrin, L., Krasnow, M.A., and Galko,  
661 M.J. (2008). Circulating blood cells function as a surveillance system for damaged tissue in  
662 Drosophila larvae. *P Natl Acad Sci USA* 105, 10017-10022.

663 Balkwill, F., and Mantovani, A. (2001). Inflammation and cancer: back to Virchow? *Lancet*  
664 357, 539-545.

665 Bartkova, J., Horejsi, Z., Koed, K., Kramer, A., Tort, F., Zieger, K., Guldberg, P., Sehested,  
666 M., Nesland, J.M., Lukas, C., *et al.* (2005). DNA damage response as a candidate anti-cancer  
667 barrier in early human tumorigenesis. *Nature* 434, 864-870.

668 Bartkova, J., Rezaei, N., Liontos, M., Karakaidos, P., Kletsas, D., Issaeva, N., Vassiliou, L.V.,  
669 Kolettas, E., Niforou, K., Zoumpourlis, V.C., *et al.* (2006). Oncogene-induced senescence is  
670 part of the tumorigenesis barrier imposed by DNA damage checkpoints. *Nature* 444, 633-637.

671 Bergmann, A., Agapite, J., McCall, K., and Steller, H. (1998). The Drosophila gene hid is a  
672 direct molecular target of Ras-dependent survival signaling. *Cell* 95, 331-341.

673 Bilder, D., Li, M., and Perrimon, N. (2000). Cooperative regulation of cell polarity and  
674 growth by Drosophila tumor suppressors. *Science* 289, 113-116.

- 675 Britton, J.S., and Edgar, B.A. (1998). Environmental control of the cell cycle in *Drosophila*:  
676 nutrition activates mitotic and endoreplicative cells by distinct mechanisms. *Development*  
677 *125*, 2149-2158.
- 678 Buchon, N., Broderick, N.A., Poidevin, M., Pradervand, S., and Lemaitre, B. (2009).  
679 *Drosophila* intestinal response to bacterial infection: activation of host defense and stem cell  
680 proliferation. *Cell Host Microbe* *5*, 200-211.
- 681 Buchon, N., Silverman, N., and Cherry, S. (2014). Immunity in *Drosophila melanogaster*--  
682 from microbial recognition to whole-organism physiology. *Nat Rev Immunol* *14*, 796-810.
- 683 Burnet, F.M. (1970). An immunological approach to ageing. *Lancet* *2*, 358-360.
- 684 Burnet, M. (1957). *Cancer - a Biological Approach* .1. The Processes of Control. *Brit Med J*  
685 *1*, 779-786.
- 686 Chatterjee, N., and Bohmann, D. (2012). A versatile PhiC31 based reporter system for  
687 measuring AP-1 and Nrf2 signaling in *Drosophila* and in tissue culture. *PLoS One* *7*, e34063.
- 688 Chovatiya, R., and Medzhitov, R. (2014). Stress, inflammation, and defense of homeostasis.  
689 *Mol Cell* *54*, 281-288.
- 690 Colombani, J., Bianchini, L., Layalle, S., Pondeville, E., Dauphin-Villemant, C.,  
691 Antoniewski, C., Carre, C., Noselli, S., and Leopold, P. (2005). Antagonistic actions of  
692 ecdysone and insulins determine final size in *Drosophila*. *Science* *310*, 667-670.
- 693 Cordero, J.B., Macagno, J.P., Stefanatos, R.K., Strathdee, K.E., Cagan, R.L., and Vidal, M.  
694 (2010). Oncogenic Ras diverts a host TNF tumor suppressor activity into tumor promoter.  
695 *Dev Cell* *18*, 999-1011.
- 696 Di Micco, R., Fumagalli, M., Cicalese, A., Piccinin, S., Gasparini, P., Luise, C., Schurra, C.,  
697 Garre, M., Nuciforo, P.G., Bensimon, A., *et al.* (2006). Oncogene-induced senescence is a  
698 DNA damage response triggered by DNA hyper-replication. *Nature* *444*, 638-642.
- 699 Edgar, B.A. (2006). How flies get their size: genetics meets physiology. *Nat Rev Genet* *7*,  
700 907-916.
- 701 Edgar, B.A., Zielke, N., and Gutierrez, C. (2014). Endocycles: a recurrent evolutionary  
702 innovation for post-mitotic cell growth (vol 15, pg 197, 2014). *Nat Rev Mol Cell Bio* *15*.
- 703 Eming, S.A. (2014). Evolution of immune pathways in regeneration and repair: recent  
704 concepts and translational perspectives. *Semin Immunol* *26*, 275-276.
- 705 Enomoto, M., Kizawa, D., Ohsawa, S., and Igaki, T. (2015). JNK signaling is converted from  
706 anti- to pro-tumor pathway by Ras-mediated switch of Warts activity. *Dev Biol* *403*, 162-171.
- 707 Fan, Y., and Bergmann, A. (2010). The cleaved-Caspase-3 antibody is a marker of Caspase-9-  
708 like DRONC activity in *Drosophila*. *Cell Death Differ* *17*, 534-539.
- 709 Ferrandon, D., Jung, A.C., Crique, M., Lemaitre, B., Uttenweiler-Joseph, S., Michaut, L.,  
710 Reichhart, J., and Hoffmann, J.A. (1998a). A drosomycin-GFP reporter transgene reveals a  
711 local immune response in *Drosophila* that is not dependent on the Toll pathway. *EMBO J* *17*,  
712 1217-1227.
- 713 Ferrandon, D., Jung, A.C., Crique, M., Lemaitre, B., Uttenweiler-Joseph, S., Michaut, L.,  
714 Reichhart, J., and Hoffmann, J.A. (1998b). A drosomycin-GFP reporter transgene reveals a  
715 local immune response in *Drosophila* that is not dependent on the Toll pathway. *Embo J* *17*,  
716 1217-1227.
- 717 Fogarty, C.E., Diwanji, N., Lindblad, J.L., Tare, M., Amcheslavsky, A., Makhijani, K.,  
718 Bruckner, K., Fan, Y., and Bergmann, A. (2016). Extracellular Reactive Oxygen Species  
719 Drive Apoptosis-Induced Proliferation via *Drosophila* Macrophages. *Curr Biol* *26*, 575-584.
- 720 Fuse, Y., and Kobayashi, M. (2017). Conservation of the Keap1-Nrf2 System: An  
721 Evolutionary Journey through Stressful Space and Time. *Molecules* *22*.
- 722 Galko, M.J., and Krasnow, M.A. (2004). Cellular and genetic analysis of wound healing in  
723 *Drosophila* larvae. *PLoS Biol* *2*, E239.



- 724 Germani, F., Hain, D., Sternlicht, D., Moreno, E., and Basler, K. (2018). The Toll pathway  
725 inhibits tissue growth and regulates cell fitness in an infection-dependent manner. *Elife* 7.  
726 Han, S.H., Ryu, J.H., Oh, C.T., Nam, K.B., Nam, H.J., Jang, I.H., Brey, P.T., and Lee, W.J.  
727 (2004). The moleskin gene product is essential for Caudal-mediated constitutive antifungal  
728 Drosomycin gene expression in *Drosophila epithelia*. *Insect Mol Biol* 13, 323-327.  
729 Hauling, T., Krautz, R., Markus, R., Volkenhoff, A., Kucerova, L., and Theopold, U. (2014).  
730 A *Drosophila* immune response against Ras-induced overgrowth. *Biol Open* 3, 250-260.  
731 Hauptmann, G. (2015). *In situ hybridization methods* (New York: Humana Press).  
732 Hawkins, C.J., Yoo, S.J., Peterson, E.P., Wang, S.L., Vernooy, S.Y., and Hay, B.A. (2000).  
733 The *Drosophila* caspase DRONC cleaves following glutamate or aspartate and is regulated by  
734 DIAP1, HID, and GRIM. *J Biol Chem* 275, 27084-27093.  
735 Hay, B.A., Wolff, T., and Rubin, G.M. (1994). Expression of Baculovirus P35 Prevents Cell-  
736 Death in *Drosophila*. *Development* 120, 2121-2129.  
737 Herranz, H., Eichenlaub, T., and Cohen, S.M. (2016). Cancer in *Drosophila*: Imaginal Discs  
738 as a Model for Epithelial Tumor Formation. *Curr Top Dev Biol* 116, 181-199.  
739 Herrera, S.C., Martin, R., and Morata, G. (2013). Tissue homeostasis in the wing disc of  
740 *Drosophila melanogaster*: immediate response to massive damage during development. *PLoS*  
741 *Genet* 9, e1003446.  
742 Herrera, S.C., and Morata, G. (2014). Transgressions of compartment boundaries and cell  
743 reprogramming during regeneration in *Drosophila*. *Elife* 3, e01831.  
744 Hoffmann, A.A., and Parsons, P.A. (1991). *Evolutionary genetics and environmental stress*  
745 (Oxford ; New York: Oxford University Press).  
746 Igaki, T., Pagliarini, R.A., and Xu, T. (2006). Loss of cell polarity drives tumor growth and  
747 invasion through JNK activation in *Drosophila*. *Curr Biol* 16, 1139-1146.  
748 Imler, J.L., and Bulet, P. (2005). Antimicrobial peptides in *Drosophila*: structures, activities  
749 and gene regulation. *Chem Immunol Allergy* 86, 1-21.  
750 Jacob, L., Oppen, M., Metzroth, B., Phannavong, B., and Mechler, B.M. (1987). Structure of  
751 the *l(2)gl* gene of *Drosophila* and delimitation of its tumor suppressor domain. *Cell* 50, 215-  
752 225.  
753 Jia, Q., Liu, Y., Liu, H., and Li, S. (2014). *Mmp1* and *Mmp2* cooperatively induce *Drosophila*  
754 fat body cell dissociation with distinct roles. *Sci Rep* 4, 7535.  
755 Junell, A., Uvell, H., Davis, M.M., Edlundh-Rose, E., Antonsson, A., Pick, L., and Engstrom,  
756 Y. (2010). The POU transcription factor Drifter/Ventral veinless regulates expression of  
757 *Drosophila* immune defense genes. *Mol Cell Biol* 30, 3672-3684.  
758 Jung, H., Hsiung, B., Pestal, K., Procyk, E., and Raulet, D.H. (2012). RAE-1 ligands for the  
759 NKG2D receptor are regulated by E2F transcription factors, which control cell cycle entry. *J*  
760 *Exp Med* 209, 2409-2422.  
761 Kholodenko, B.N. (2006). Cell-signalling dynamics in time and space. *Nat Rev Mol Cell Biol*  
762 7, 165-176.  
763 Kim, M.J., and Choe, K.M. (2014). Basement membrane and cell integrity of self-tissues in  
764 maintaining *Drosophila* immunological tolerance. *PLoS Genet* 10, e1004683.  
765 Kurada, P., and White, K. (1998). Ras promotes cell survival in *Drosophila* by  
766 downregulating *hid* expression. *Cell* 95, 319-329.  
767 Kurata, S. (2004). Recognition of infectious non-self and activation of immune responses by  
768 peptidoglycan recognition protein (PGRP)-family members in *Drosophila*. *Developmental*  
769 *and Comparative Immunology* 28, 89-95.  
770 Lemaitre, B., and Hoffmann, J. (2007). The host defense of *Drosophila melanogaster*. *Annu*  
771 *Rev Immunol* 25, 697-743.

- 772 Liu, D., Shaukat, Z., Saint, R.B., and Gregory, S.L. (2015). Chromosomal instability triggers  
773 cell death via local signalling through the innate immune receptor Toll. *Oncotarget* 6, 38552-  
774 38565.
- 775 Loboda, A., Damulewicz, M., Pyza, E., Jozkowicz, A., and Dulak, J. (2016). Role of  
776 Nrf2/HO-1 system in development, oxidative stress response and diseases: an evolutionarily  
777 conserved mechanism. *Cell Mol Life Sci* 322, 3221-3247.
- 778 Lowe, S.W., Cepero, E., and Evan, G. (2004). Intrinsic tumour suppression. *Nature* 432, 307-  
779 315.
- 780 Mantovani, A., Allavena, P., Sica, A., and Balkwill, F. (2008). Cancer-related inflammation.  
781 *Nature* 454, 436-444.
- 782 Mason, D.X., Jackson, T.J., and Lin, A.W. (2004). Molecular signature of oncogenic ras-  
783 induced senescence. *Oncogene* 23, 9238-9246.
- 784 Medzhitov, R., and Janeway, C.A. (2002). Decoding the patterns of self and nonself by the  
785 innate immune system. *Science* 296, 298-300.
- 786 Meier, P., Silke, J., Leever, S.J., and Evan, G.I. (2000). The *Drosophila* caspase DRONC is  
787 regulated by DIAP1. *EMBO J* 19, 598-611.
- 788 Meyer, S.N., Amoyel, M., Bergantinos, C., de la Cova, C., Schertel, C., Basler, K., and  
789 Johnston, L.A. (2014). An ancient defense system eliminates unfit cells from developing  
790 tissues during cell competition. *Science* 346, 1258236.
- 791 Mirth, C.K., Tang, H.Y., Makohon-Moore, S.C., Salhadar, S., Gokhale, R.H., Warner, R.D.,  
792 Koyama, T., Riddiford, L.M., and Shingleton, A.W. (2014). Juvenile hormone regulates body  
793 size and perturbs insulin signaling in *Drosophila*. *Proc Natl Acad Sci U S A* 111, 7018-7023.
- 794 Morin, X., Daneman, R., Zavortink, M., and Chia, W. (2001). A protein trap strategy to detect  
795 GFP-tagged proteins expressed from their endogenous loci in *Drosophila*. *Proc Natl Acad Sci*  
796 *U S A* 98, 15050-15055.
- 797 Muzzopappa, M., Murcia, L., and Milan, M. (2017). Feedback amplification loop drives  
798 malignant growth in epithelial tissues. *Proc Natl Acad Sci U S A* 114, E7291-E7300.
- 799 Ohlstein, B., and Spradling, A. (2006). The adult *Drosophila* posterior midgut is maintained  
800 by pluripotent stem cells. *Nature* 439, 470-474.
- 801 Orr-Weaver, T.L. (2015). When bigger is better: the role of polyploidy in organogenesis.  
802 *Trends Genet* 31, 307-315.
- 803 Pagliarini, R.A., and Xu, T. (2003). A genetic screen in *Drosophila* for metastatic behavior.  
804 *Science* 302, 1227-1231.
- 805 Parisi, F., Stefanatos, R.K., Strathdee, K., Yu, Y., and Vidal, M. (2014). Transformed  
806 epithelia trigger non-tissue-autonomous tumor suppressor response by adipocytes via  
807 activation of Toll and Eiger/TNF signaling. *Cell Rep* 6, 855-867.
- 808 Park, J.M., Brady, H., Ruocco, M.G., Sun, H., Williams, D., Lee, S.J., Kato, T., Jr., Richards,  
809 N., Chan, K., Mercurio, F., *et al.* (2004). Targeting of TAK1 by the NF-kappa B protein  
810 Relish regulates the JNK-mediated immune response in *Drosophila*. *Genes Dev* 18, 584-594.
- 811 Parvy, J.P., Yu, Y., Dostalova, A., Kondo, S., Kurjan, A., Bulet, P., Lemaitre, B., Vidal, M.,  
812 and Cordero, J.B. (2019). The antimicrobial peptide Defensin cooperates with Tumor  
813 Necrosis Factor to drive tumour cell death in *Drosophila*. *BioRxiv*.
- 814 Pastor-Pareja, J.C., Wu, M., and Xu, T. (2008). An innate immune response of blood cells to  
815 tumors and tissue damage in *Drosophila*. *Dis Model Mech* 1, 144-154; discussion 153.
- 816 Perez, E., Lindblad, J.L., and Bergmann, A. (2017). Tumor-promoting function of apoptotic  
817 caspases by an amplification loop involving ROS, macrophages and JNK in *Drosophila*. *Elife*  
818 6.
- 819 Pinal, N., Martin, M., Medina, I., and Morata, G. (2018). Short-term activation of the Jun N-  
820 terminal kinase pathway in apoptosis-deficient cells of *Drosophila* induces tumorigenesis. *Nat*  
821 *Commun* 9, 1541.



822 Piper, M.D., Blanc, E., Leitao-Goncalves, R., Yang, M., He, X., Linford, N.J., Hoddinott,  
823 M.P., Hopfen, C., Soultoukis, G.A., Niemeyer, C., *et al.* (2014). A holidic medium for  
824 *Drosophila melanogaster*. *Nat Methods* *11*, 100-105.

825 Rämét, M., Lanot, R., Zachary, D., and Manfrulli, P. (2002). JNK signaling pathway is  
826 required for efficient wound healing in *Drosophila*. *Dev Biol* *241*, 145-156.

827 Ramos-Lewis, W., and Page-McCaw, A. (2019). Basement membrane mechanics shape  
828 development: Lessons from the fly. *Matrix Biology* *75-76*, 72-81.

829 Rankin, L.C., and Artis, D. (2018). Beyond Host Defense: Emerging Functions of the  
830 Immune System in Regulating Complex Tissue Physiology. *Cell* *173*, 554-567.

831 Ryu, J.H., Kim, S.H., Lee, H.Y., Bai, J.Y., Nam, Y.D., Bae, J.W., Lee, D.G., Shin, S.C., Ha,  
832 E.M., and Lee, W.J. (2008). Innate immune homeostasis by the homeobox gene *caudal* and  
833 commensal-gut mutualism in *Drosophila*. *Science* *319*, 777-782.

834 Ryu, J.H., Nam, K.B., Oh, C.T., Nam, H.J., Kim, S.H., Yoon, J.H., Seong, J.K., Yoo, M.A.,  
835 Jang, I.H., Brey, P.T., *et al.* (2004). The homeobox gene *Caudal* regulates constitutive local  
836 expression of antimicrobial peptide genes in *Drosophila* epithelia. *Mol Cell Biol* *24*, 172-185.

837 Santabarbara-Ruiz, P., Lopez-Santillan, M., Martinez-Rodriguez, I., Binagui-Casas, A., Perez,  
838 L., Milan, M., Corominas, M., and Serras, F. (2015). ROS-Induced JNK and p38 Signaling Is  
839 Required for Unpaired Cytokine Activation during *Drosophila* Regeneration. *PLoS Genet* *11*,  
840 e1005595.

841 Schmiedel, D., and Mandelboim, O. (2018). NKG2D Ligands-Critical Targets for Cancer  
842 Immune Escape and Therapy. *Front Immunol* *9*, 2040.

843 Schuster, K.J., and Smith-Bolton, R.K. (2015). *Taranis* Protects Regenerating Tissue from  
844 Fate Changes Induced by the Wound Response in *Drosophila*. *Dev Cell* *34*, 119-128.

845 Shim, J. (2015). *Drosophila* blood as a model system for stress sensing mechanisms. *Bmb*  
846 *Rep* *48*, 223-228.

847 Shim, J., Gururaja-Rao, S., and Banerjee, U. (2013). Nutritional regulation of stem and  
848 progenitor cells in *Drosophila*. *Development* *140*, 4647-4656.

849 Shlevkov, E., and Morata, G. (2012). A *dp53*/JNK-dependant feedback amplification loop is  
850 essential for the apoptotic response to stress in *Drosophila*. *Cell Death Differ* *19*, 451-460.

851 Smith, A.V., and Orr-Weaver, T.L. (1991). The regulation of the cell cycle during *Drosophila*  
852 embryogenesis: the transition to polyteny. *Development* *112*, 997-1008.

853 Sorrentino, R.P. (2010). Large standard deviations and logarithmic-normality: the truth about  
854 hemocyte counts in *Drosophila*. *Fly (Austin)* *4*, 327-332.

855 Stevens, L.J., and Page-McCaw, A. (2012). A secreted MMP is required for  
856 reepithelialization during wound healing. *Mol Biol Cell* *23*, 1068-1079.

857 Strand, D., Jakobs, R., Merdes, G., Neumann, B., Kalmes, A., Heid, H.W., Husmann, I., and  
858 Mechler, B.M. (1994). The *Drosophila* *Lethal(2)Giant Larvae Tumor-Suppressor Protein*  
859 *Forms Homo-Oligomers and Is Associated with Nonmuscle Myosin-Ii Heavy-Chain*. *Journal*  
860 *of Cell Biology* *127*, 1361-1373.

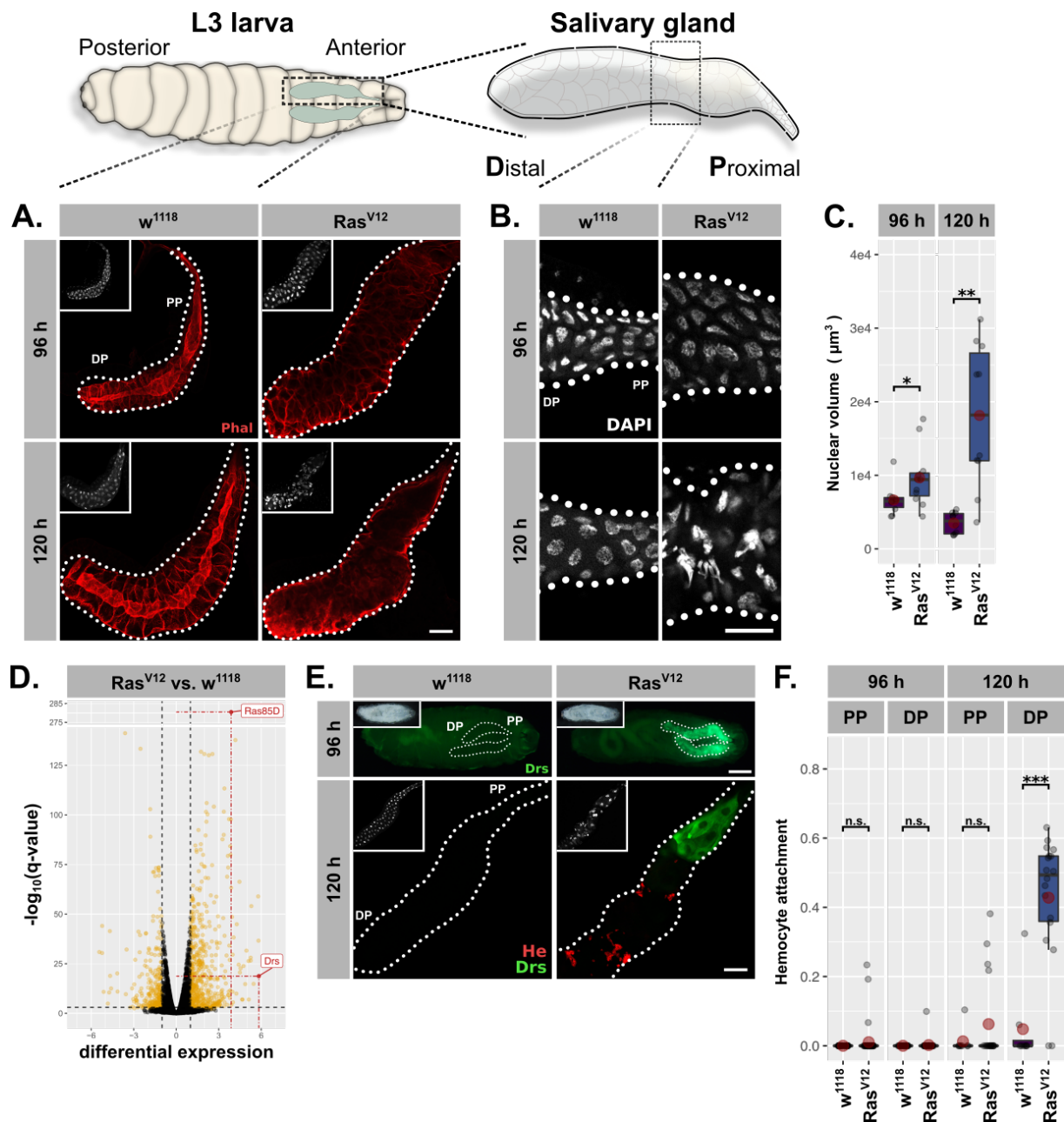
861 Stronach, B.E., and Perrimon, N. (1999). Stress signaling in *Drosophila*. *Oncogene* *18*, 6172-  
862 6182.

863 Takehana, A., Yano, T., Mita, S., Kotani, A., Oshima, Y., and Kurata, S. (2004).  
864 Peptidoglycan recognition protein (PGRP)-LE and PGRP-LC act synergistically in  
865 *Drosophila* immunity. *Embo J* *23*, 4690-4700.

866 Y. Tamori, W. M. Deng, Compensatory cellular hypertrophy: the other strategy for  
867 tissuehomeostasis, *Trends Cell Biol* *24*(2014) 230-237.

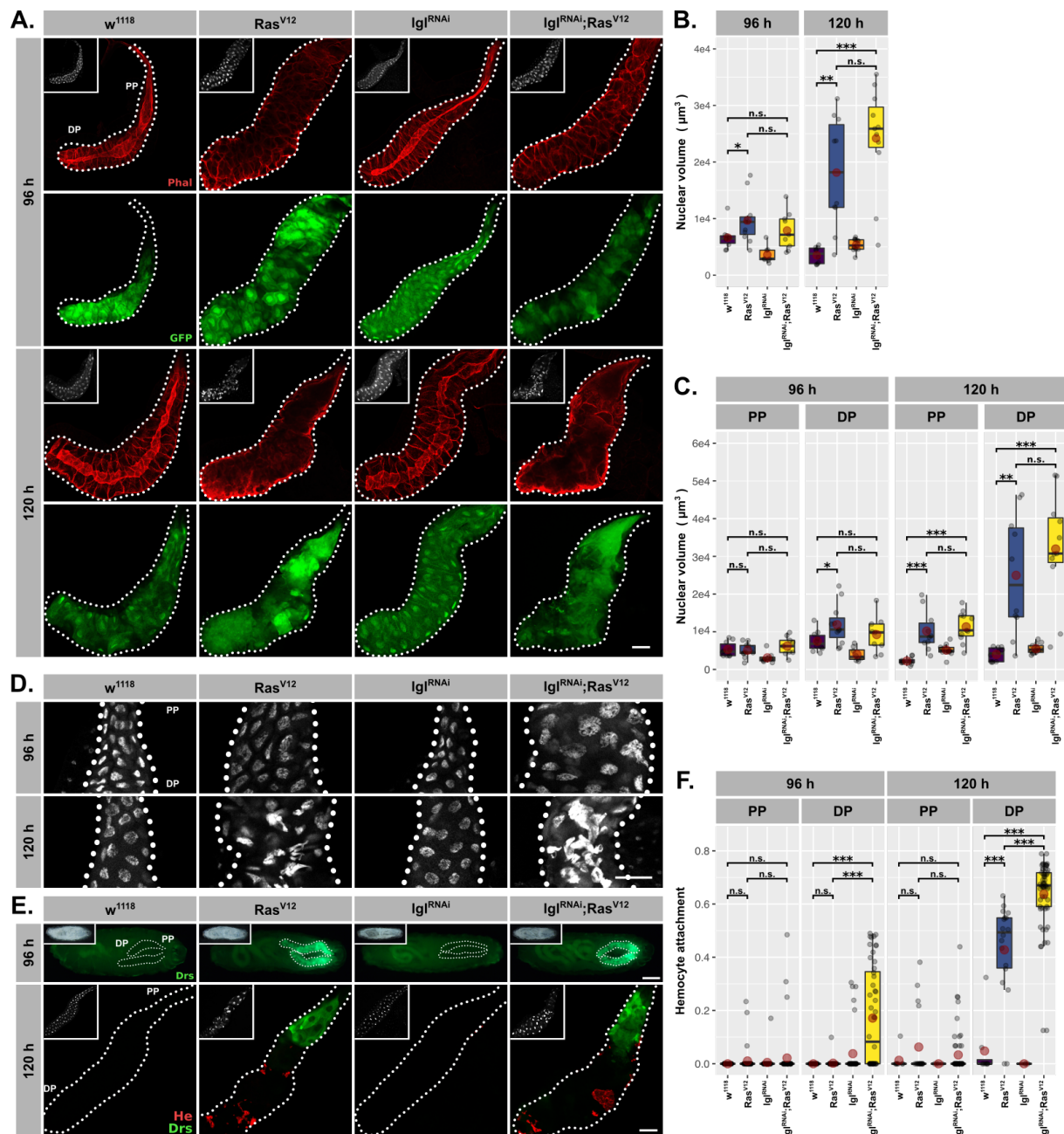
868 Tzou, P., Ohresser, S., Ferrandon, D., Capovilla, M., Reichhart, J.M., Lemaitre, B.,  
869 Hoffmann, J.A., and Imler, J.L. (2000). Tissue-specific inducible expression of antimicrobial  
870 peptide genes in *Drosophila* surface epithelia. *Immunity* *13*, 737-748.

- 871 Uhlirova, M., and Bohmann, D. (2006). JNK- and Fos-regulated Mmp1 expression cooperates  
872 with Ras to induce invasive tumors in *Drosophila*. *Embo J* 25, 5294-5304.
- 873 Uhlirova, M., Jasper, H., and Bohmann, D. (2005). Non-cell-autonomous induction of tissue  
874 overgrowth by JNK/Ras cooperation in a *Drosophila* tumor model. *Proc Natl Acad Sci U S A*  
875 102, 13123-13128.
- 876 Vantourout, P., Willcox, C., Turner, A., Swanson, C.M., Haque, Y., Sobolev, O., Grigoriadis,  
877 A., Tutt, A., and Hayday, A. (2014). Immunological visibility: posttranscriptional regulation  
878 of human NKG2D ligands by the EGF receptor pathway. *Sci Transl Med* 6, 231ra249.
- 879 Vermeulen, C.J., and Loeschcke, V. (2007). Longevity and the stress response in *Drosophila*.  
880 *Exp Gerontol* 42, 153-159.
- 881 Vidal, M. (2010). The dark side of fly TNF: an ancient developmental proof reading  
882 mechanism turned into tumor promoter. *Cell Cycle* 9, 3851-3856.
- 883 Wagner, C., Isermann, K., and Roeder, T. (2009). Infection induces a survival program and  
884 local remodeling in the airway epithelium of the fly. *FASEB J* 23, 2045-2054.
- 885 Wu, C., Chen, C., Dai, J., Zhang, F., Chen, Y., Li, W., Pastor-Pareja, J.C., and Xue, L. (2015).  
886 Toll pathway modulates TNF-induced JNK-dependent cell death in *Drosophila*. *Open Biol* 5,  
887 140171.  
888



889

890 **Figure 1. *Ras<sup>V12</sup>*-induced hypertrophy induces local and systemic immune responses** (A.) *Ras<sup>V12</sup>*-glands and  
891 controls stained with Phalloidin (red) to monitor tissue integrity at 96 h and 120 h AED. (B.) Nuclei stained with  
892 DAPI (white) to visualize nuclear volume and disintegration at 120 h AED in *Ras<sup>V12</sup>*-glands. (C.) Nuclear volume  
893 as quantified by z-stacks of DAPI-stained SGs at 96 h and 120 h AED and averaged per gland. (D.) Comparative  
894 transcriptome analysis of *Ras<sup>V12</sup>*-vs.-*w<sup>1118</sup>*-glands. Differential expression quantified as beta statistic with q-values  
895 by wald test. Significantly differentially expressed genes ( $\log_2(\text{beta}) \geq 1$ ;  $q\text{-value} \leq 0.05$ ) highlighted in yellow. (E.)  
896 Upper: Whole larvae with DrsGFP reporter (green) expressing *Ras<sup>V12</sup>* in glands or controls at 96 h AED. Lower:  
897 *Ras<sup>V12</sup>*- and control-glands with DrsGFP reporter (green) stained for hemocytes (anti-Hemese, red). (F.) Hemocyte  
898 attachment measured as  $\ln(\text{Hemese-area})/\ln(\text{SG-area})$  and separated by time and gland part. Insets: (A./E. Lower)  
899 DAPI, (E. Upper) brightfield. Scalebars: (A./B./E. Lower) 100  $\mu\text{m}$ , (E. Upper) 500  $\mu\text{m}$ . Boxplots in (C./F.):  
900 lower/upper hinges indicate 1<sup>st</sup>/3<sup>rd</sup> quartiles, whisker lengths equal 1.5\*IQR, red circle and bar represent mean and  
901 median. Significance evaluated by Student's t-tests (\*\*\*)  $p < 0.001$ , \*\*  $p < 0.01$ , \*  $p < 0.05$ , n.s.  $p \geq 0.05$ ).

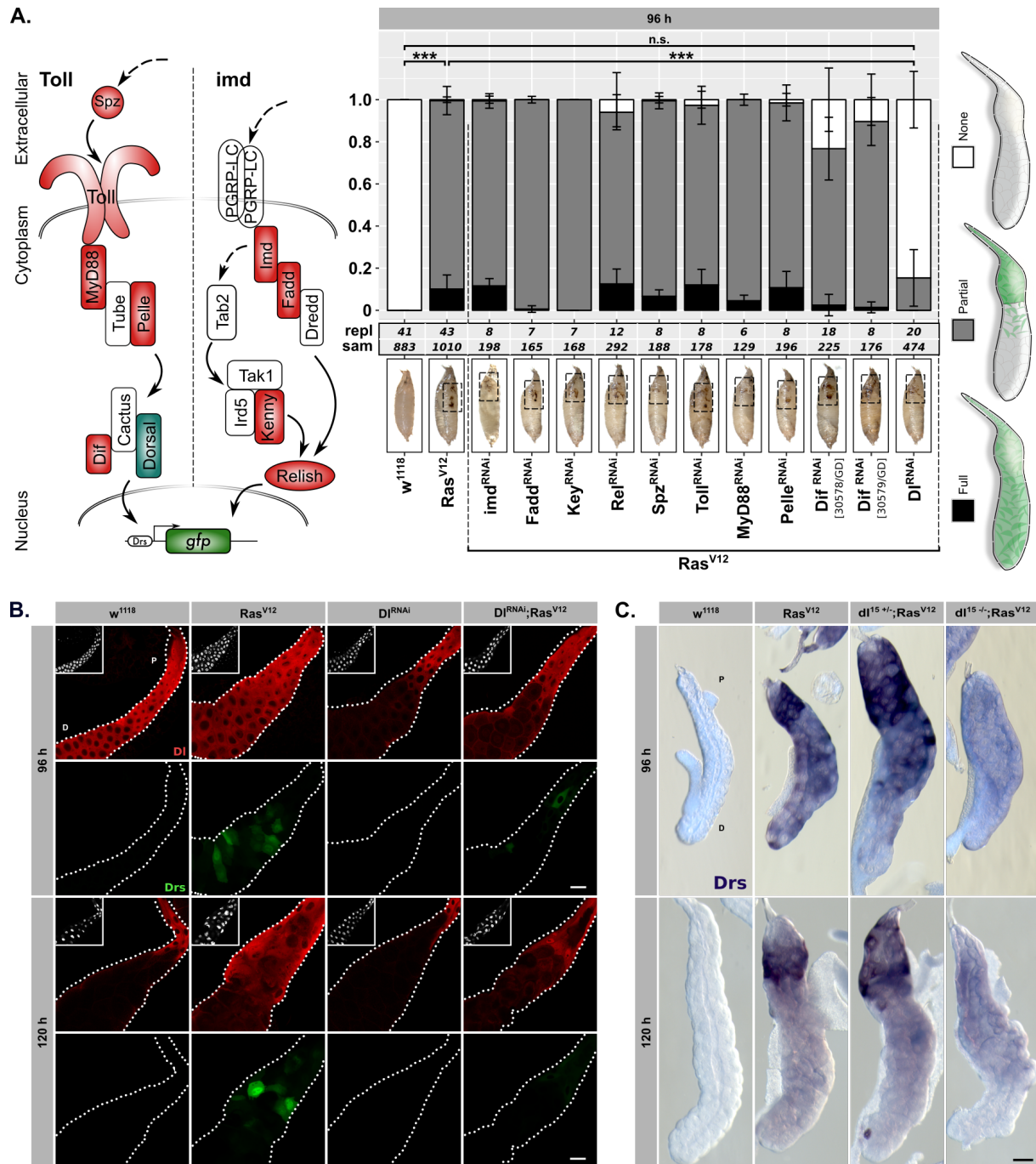


902

903 **Supplemental Figure 1.** (A.) GFP (green) expression to validate *Bx<sup>MS1096</sup>* driver at 96 h and 120 h AED in all  
 904 genotypes and Phalloidin (red) staining to trace tissue integrity. (B.) Volume of DAPI-stained nuclei derived from  
 905 SG z-stacks and averaged per gland. (C.) Nuclear volume separated per gland into DP and PP. (D.) SG nuclei  
 906 stained with DAPI (white) to indicate nuclear size and disintegration. (E.) Upper: Whole larvae carrying DrsGFP  
 907 reporter (green). Lower: SGs with DrsGFP reporter signal (green) and stained hemocytes (anti-Hemese, red). (F.)  
 908 Attached hemocytes quantified as  $\ln(\text{Hemese-area})/\ln(\text{SG-area})$  separated for DP and PP. Insets: (A./E. Lower)  
 909 DAPI, (E. Upper) brightfield. Scalebars: (A./D./E. Lower) 100  $\mu\text{m}$ , (E. Upper) 500  $\mu\text{m}$ . Boxplots in (B./C./F.):  
 910 lower/upper hinges indicate 1<sup>st</sup>/3<sup>rd</sup> quartiles, whisker lengths equal 1.5\*IQR, red circle and bar represent mean and  
 911 median. Significance evaluated by Student's t-tests (\*\*\*)  $p < 0.001$ , (\*\*)  $p < 0.01$ , (\*)  $p < 0.05$ , n.s.  $p \geq 0.05$ . (A.-B./D.-  
 912 E.) *w<sup>1118</sup>* and *Ras<sup>V12</sup>* data reused from Fig1. (C.) Separated nuclei measurements based on data in (B.). (F.)  
 913 Separated hemocyte attachment measurements based on data in Fig1F.

914





915

916

917

918

919

920

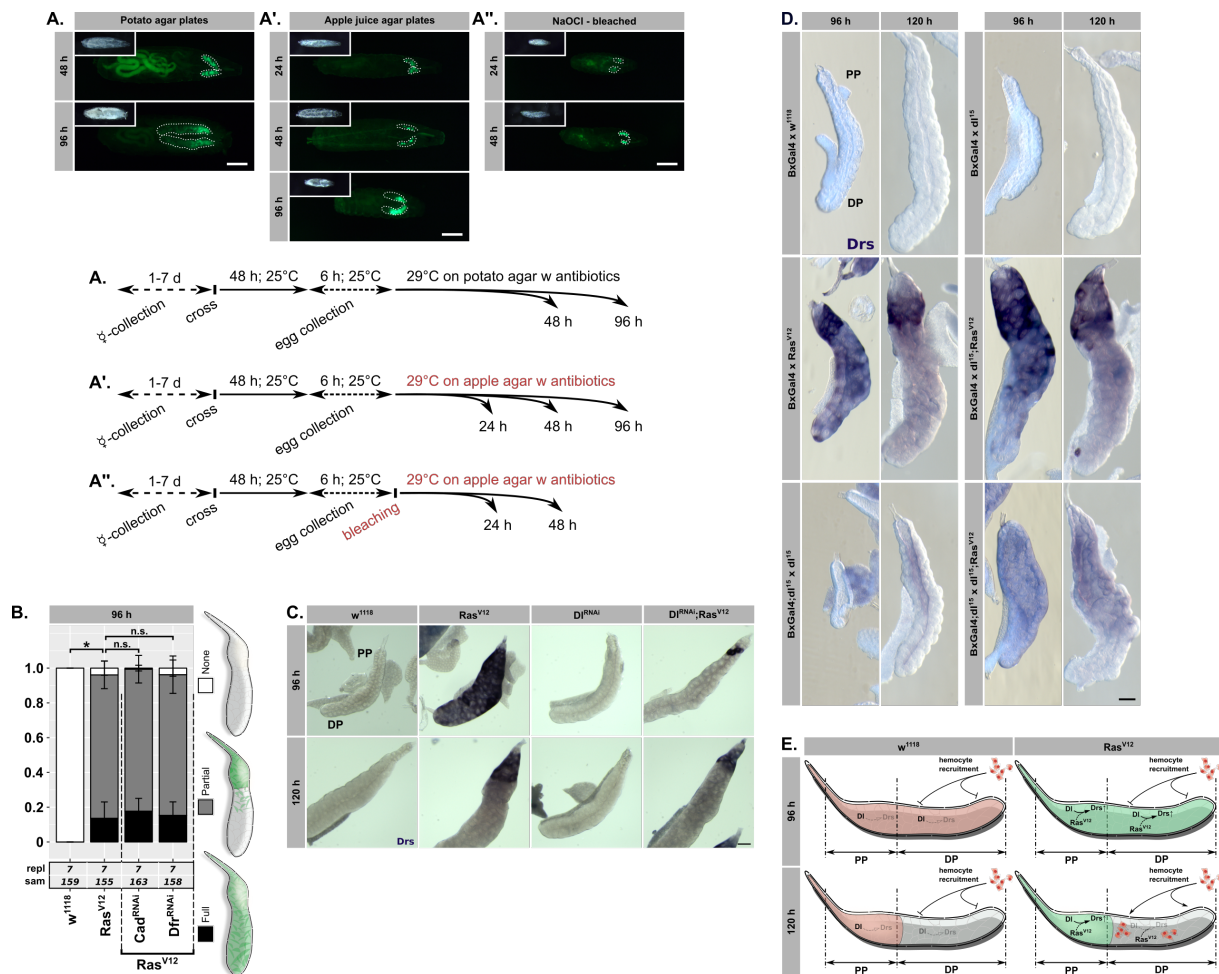
921

922

923

924

925



926

927 **Supplemental Figure 2.** Larvae with Ras<sup>V12</sup>-glands and DrsGFP reporter (green) (A.) raised on plates with

928 standard potatomash/molasses medium including stringent antibiotics cocktail, (A.') transferred immediately after

929 hatching to germ- and yeast-extract free apple-agar supplemented with antibiotics or (A.'') after egg

930 dechorionization were raised on sterile apple-agar including antibiotics. (B.) DrsGFP reporter assay with RNAi

931 constructs against Caudal and Drifter in Ras<sup>V12</sup>-glands. Sketched phenotypes (right) were scored, their mean and

932 standard deviations plotted. Dunn's test performed to evaluate significant differences in distribution of "None"-

933 phenotype (\*  $p < 0.05$ , n.s.  $p \geq 0.05$ ). (C.) Endogenous Drs mRNA detected by *in-situ* hybridization in Ras<sup>V12</sup>-glands

934 with or without knocking down Dorsal. (D.) Complete set of experimental genotypes for Drs *in-situ* hybridization

935 as shown in Fig2C including additional controls. (E.) Schematic representation of endogenous, spatio-temporally

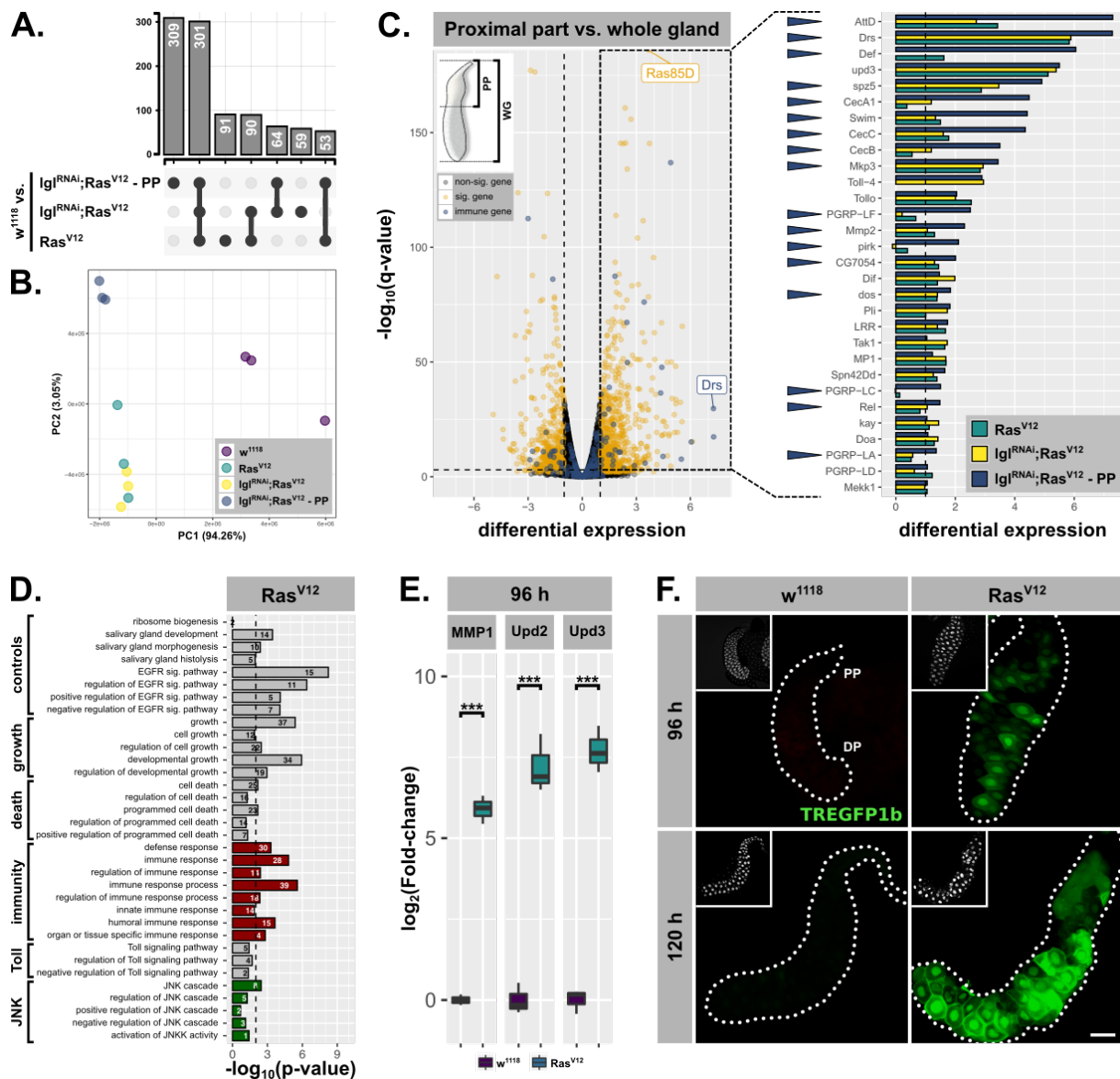
936 regulated Dorsal expression pattern in SGs and its interaction with Ras<sup>V12</sup> to promote Drs expression. Separation

937 of Ras<sup>V12</sup>-glands becomes apparent at 120 h AED with Drs-expression in PP and hemocyte recruitment to DP

938 surface.

939





940

941 **Figure 3. Hypertrophic *Ras<sup>V12</sup>*-glands induce parallel immune and stress responses (A.) Common and specific**

942 **genesets significantly upregulated ( $\log_2(\beta) \geq 1$ ;  $q\text{-value} \leq 0.05$ ) in either *Ras<sup>V12</sup>*, *IgI<sup>RNAi</sup>;Ras<sup>V12</sup>* or *IgI<sup>RNAi</sup>;Ras<sup>V12</sup>-***

943 **PP compared to *w<sup>1118</sup>*-glands. (B.) PCA including all transcriptome replicates of all sequenced genotypes. (C.) Left:**

944 **Comparative transcriptome analysis between PP of *IgI<sup>RNAi</sup>;Ras<sup>V12</sup>*- and entire *w<sup>1118</sup>*-glands. Significantly**

945 **differentially expressed genes ( $\log_2(\beta) \geq 1$ ;  $q\text{-value} \leq 0.05$ ) and genes belonging to GO-term ‘immune response’**

946 **(GO:0006955) highlighted in yellow and blue. Right: Gene expression in *Ras<sup>V12</sup>*, *IgI<sup>RNAi</sup>;Ras<sup>V12</sup>* or *IgI<sup>RNAi</sup>;Ras<sup>V12</sup>-***

947 **PP compared to *w<sup>1118</sup>*-glands for immune genes significantly upregulated in the PP. Blue arrows indicate strongest**

948 **expression in the PP for the indicated genes between all three groups. (D.) GO term enrichment among**

949 **significantly upregulated genes in *Ras<sup>V12</sup>*-glands including terms related to activation of JNK (green) and immune**

950 **responses (red). Numbers in bars indicate amount of upregulated genes belonging to associated GO term. (E.)**

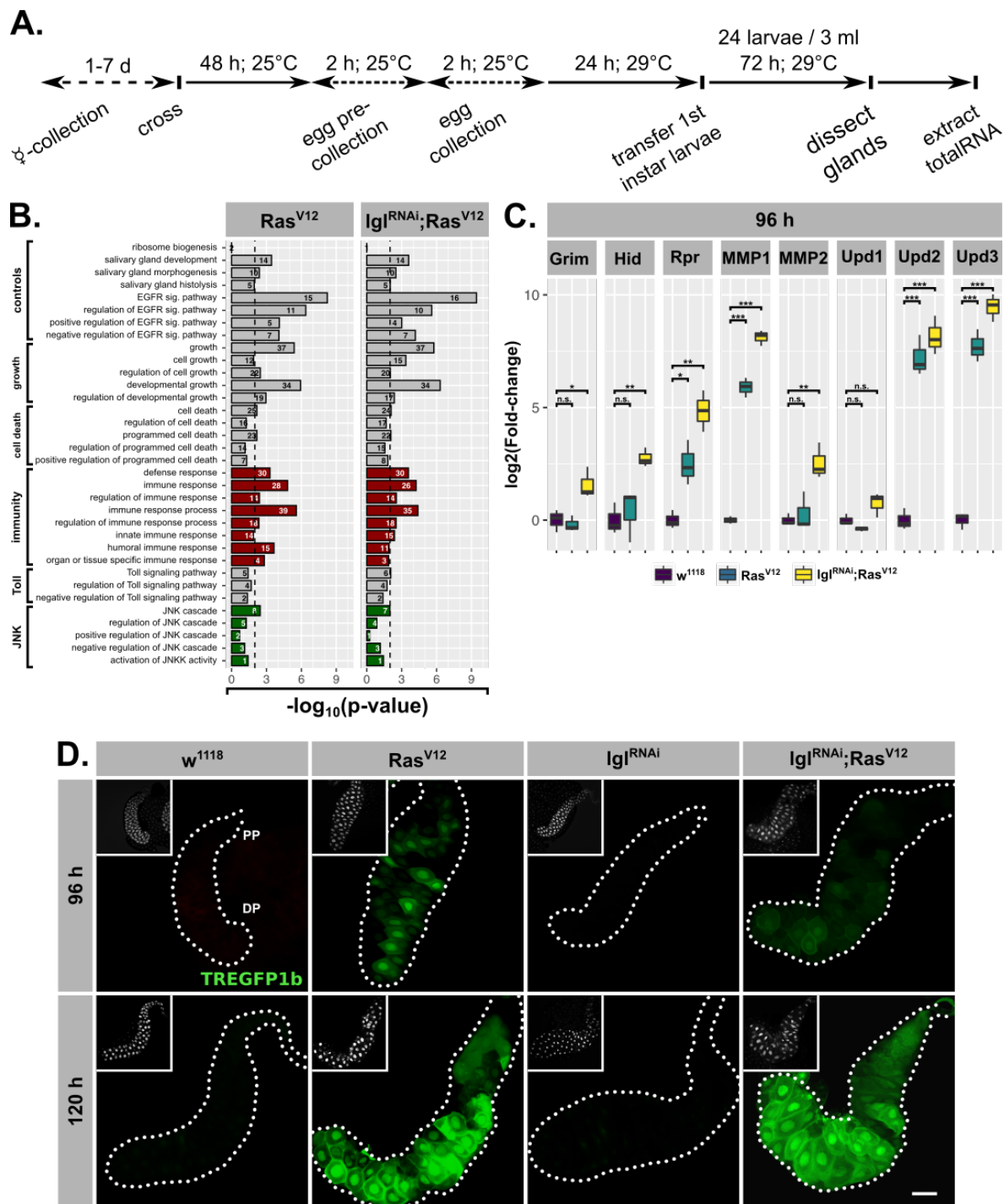
951 **qPCR results for canonical JNK target genes ( $\log_2$ -transformed, fold-change over *RpI32*) at 96 h AED.**

952 **Lower/upper hinges of boxplots indicate 1<sup>st</sup>/3<sup>rd</sup> quartiles, whisker lengths equal 1.5\*IQR and bar represents median.**

953 **Significance evaluated by Student's t-tests (\*\*\*)  $p < 0.001$ . (F.) TREGFP1b reporter (green) signal in *Ras<sup>V12</sup>*- and**

954 **control-glands at 96 h and 120 h AED. Scalbar: 100  $\mu\text{m}$ .**

955



956

957 **Supplemental Figure 3.** (A.) Schematic overview of protocol for preparing tissues analysed by RNAseq. (B.)

958 Comparative GO term enrichment analysis for genes significantly upregulated in either *Ras<sup>V12</sup>*- or *Igl<sup>RNAi</sup>;Ras<sup>V12</sup>*-

959 glands. Terms associated with activation of JNK (green) or immune response (red) are highlighted. GO terms for

960 *Ras<sup>V12</sup>* also shown in Fig3D. (C.) Gene expression for canonical target genes measured by qPCR ( $\log_2$ -transformed,

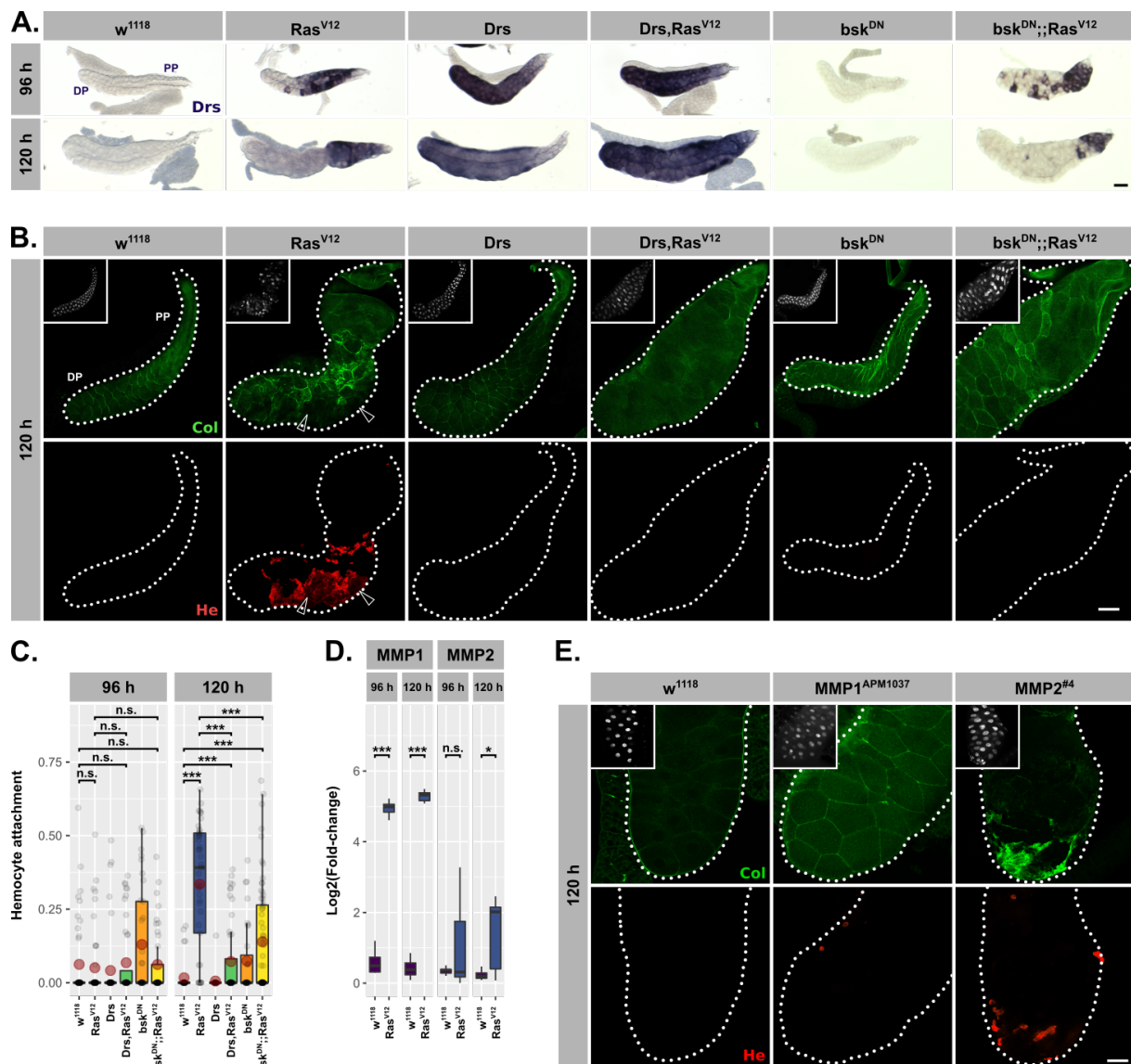
961 fold-change over *Rpl32*). Lower/upper hinges of boxplots indicate 1<sup>st</sup>/3<sup>rd</sup> quartiles, whisker lengths equal 1.5\*IQR

962 and bar represents median. Significance evaluated by Student's t-tests (\*\*\*)  $p < 0.001$ , \*\*  $p < 0.01$ , \*  $p < 0.05$ , n.s.

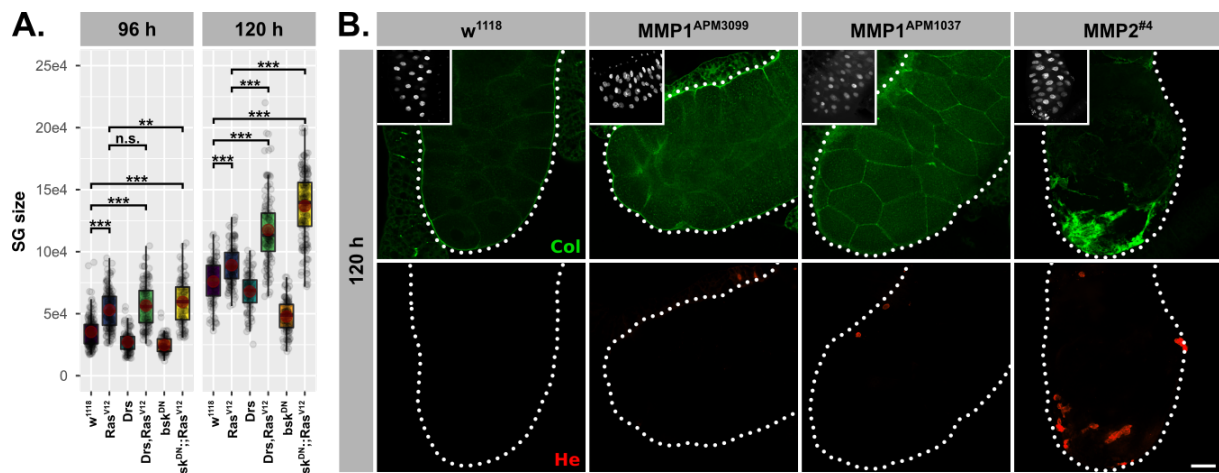
963  $p \geq 0.05$ ). Results for MMP1, Upd2 and Upd3 in *Ras<sup>V12</sup>*- and *w<sup>1118</sup>*-glands also presented in Fig3E. (D.) Activation

964 of TREGFP1b reporter (green) used to evaluate induction of JNK-signalling at 96 h and 120 h AED. *Ras<sup>V12</sup>*- and

965 *w<sup>1118</sup>*-images also presented in Fig3F. Scalebar: 100  $\mu$ m.



966  
 967 **Figure 4. Drs overexpression and JNK inhibition individually prevent tissue disintegration** (A.) Drs-specific  
 968 *in-situ* hybridization identifies endogenous (*Ras<sup>V12</sup> / bsk<sup>DN</sup>;Ras<sup>V12</sup>*) and exogenous (*Drs / Drs,Ras<sup>V12</sup>*) Drs  
 969 expression. (B.) Collagen-GFP trap (*vkg<sup>G00454</sup>*, green) and Hemese staining (red) identify integrity of BM and  
 970 hemocyte attachment to gland surface. Arrows indicate BM-free areas occupied by hemocytes. (C.) Hemocyte  
 971 attachment at 96 h and 120 h AED represented as  $\ln(\text{Hemese-area})/\ln(\text{SG-area})$ . (D.)  $\log_2$ -transformed, *Rpl32*-  
 972 normalized gene expression values obtained by qPCR at 96 h and 120 h AED. (E.) Visualization of BM by  
 973 Collagen-GFP trap (green) and Hemese-stained hemocytes (red) attached to the gland surface upon sole MMP1-  
 974 or MMP2-overexpression. Insets: (B./E.) DAPI. Scalebars: (A./B./E.) 100  $\mu\text{m}$ . Boxplots in (C./D.): lower/upper  
 975 hinges indicate 1<sup>st</sup>/3<sup>rd</sup> quartiles, whisker lengths equal 1.5\*IQR, red circle and bar represent mean and median.  
 976 Significance evaluated by Student's t-tests (\*\* $p < 0.001$ , \* $p < 0.01$ , \* $p < 0.05$ , *n.s.*  $p \geq 0.05$ ).  
 977



978

979 **Supplemental Figure 4.** (A.) SG size measured as outlined area in captured images at 96 h and 120 h AED.

980 Lower/upper hinges of boxplots indicate 1<sup>st</sup>/3<sup>rd</sup> quartiles, whisker lengths equal 1.5\*IQR, red circle and bar

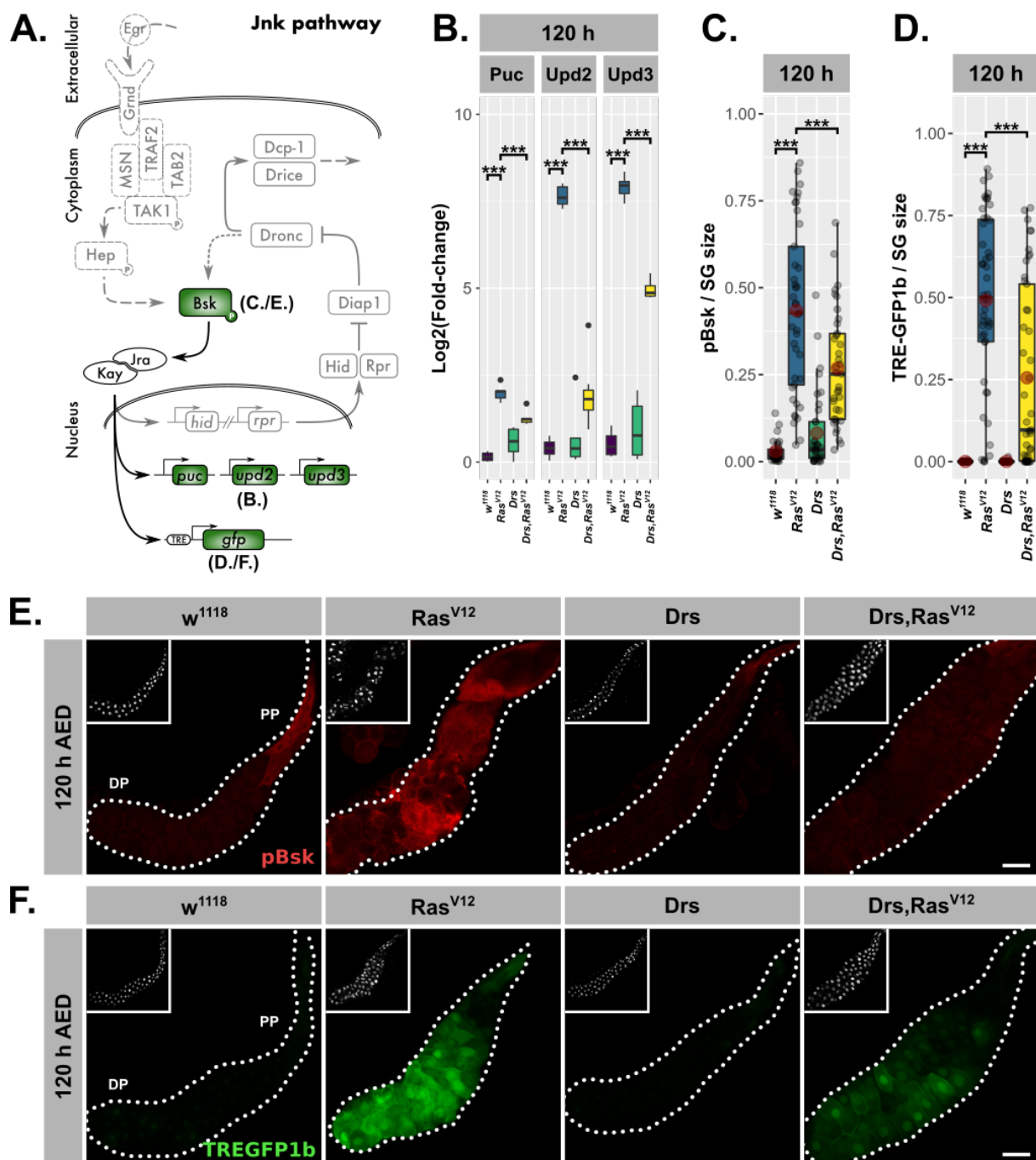
981 represent mean and median. Significance evaluated by Student's t-tests (\*\*\*)  $p < 0.001$ , \*\*  $p < 0.01$ , \*  $p < 0.05$ , n.s.

982  $p \geq 0.05$ ). (B.) Staining of BM via Collagen-GFP trap and attached hemocytes via Hemese antibody upon MMP1-

983 or MMP2-overexpression. Images for  $MMP1^{APM1037}$  and  $MMP2^{#4}$  shown in Fig4E. Scalebar represents 100  $\mu m$

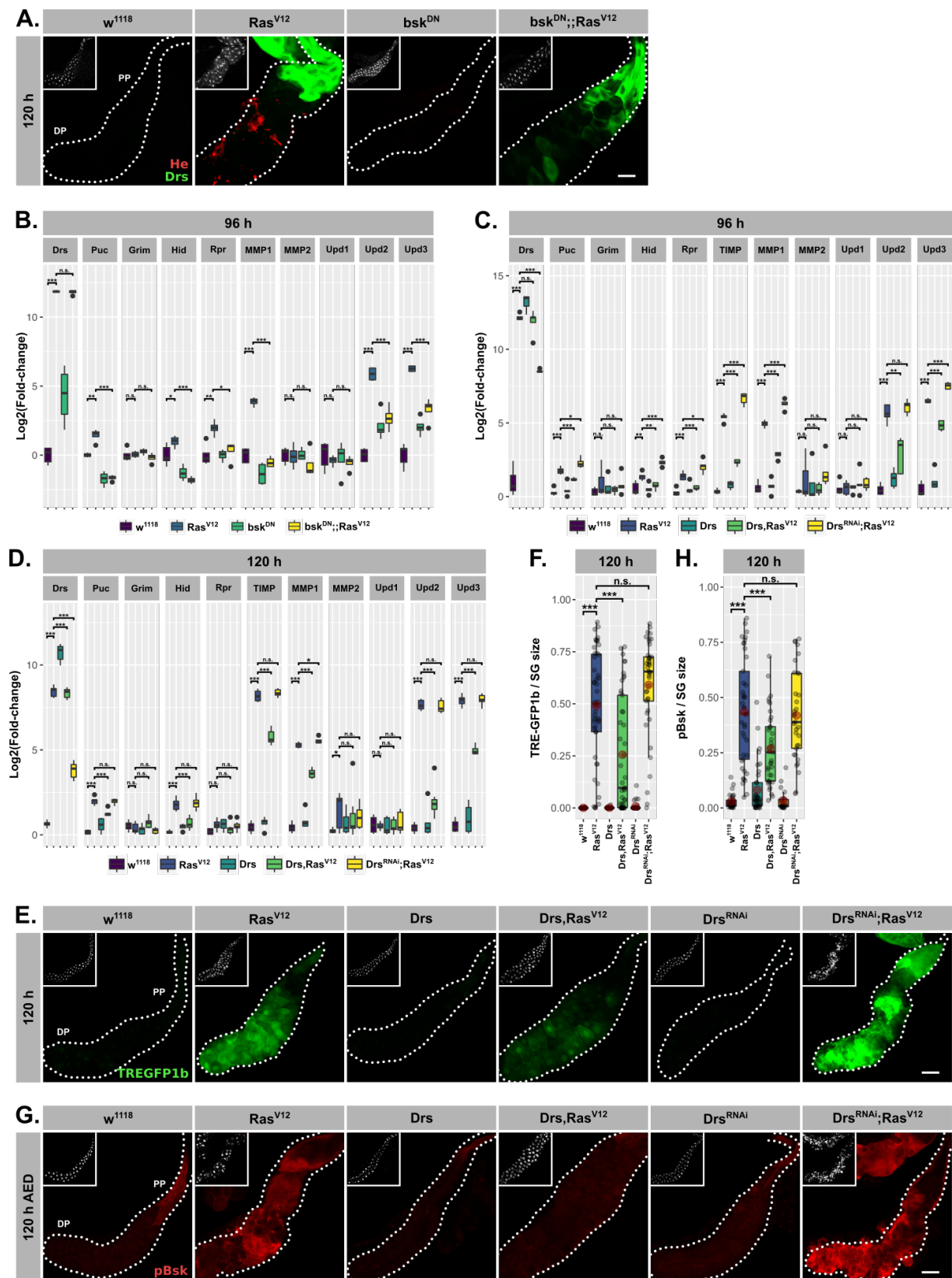
984 and insets show DAPI staining.

985



986  
 987 **Figure 5. Drs overexpression inhibits JNK-activation** (A.) Schematic representation of the JNK-pathway  
 988 including read-outs (green) employed to track its activation. (B.) qPCR results for canonical JNK-target genes  
 989 (*log<sub>2</sub>*-transformed, fold-change over *Rpl32*) at 120 h AED. (C.) Quantification of activated basket by staining with  
 990 phosphorylation sensitive antibody per gland normalized for the SG size at 120 h AED. (D.) Quantification of  
 991 TREGFP1b signal per gland normalized for SG size indicating JNK-dependent transcriptional activation at 120 h  
 992 AED. (E.) Visualization of phosphorylated basket in *Ras<sup>V12</sup>*-glands with and without Drs coexpression. (F.)  
 993 Distribution of TREGFP1b reporter signal in *Ras<sup>V12</sup>*-glands in the presence or absence of coexpressed Drs. Insets:  
 994 (E./F.) DAPI. Scalebars: (E./F.) 100  $\mu$ m. Boxplots in (B./C./D.): lower/upper hinges indicate 1<sup>st</sup>/3<sup>rd</sup> quartiles,  
 995 whisker lengths equal 1.5\*IQR, red circle and bar represent mean and median. Significance evaluated by Student's  
 996 t-tests (\*\* $p < 0.001$ , \*\*  $p < 0.01$ , \*  $p < 0.05$ , n.s.  $p \geq 0.05$ ).  
 997





998

999

1000

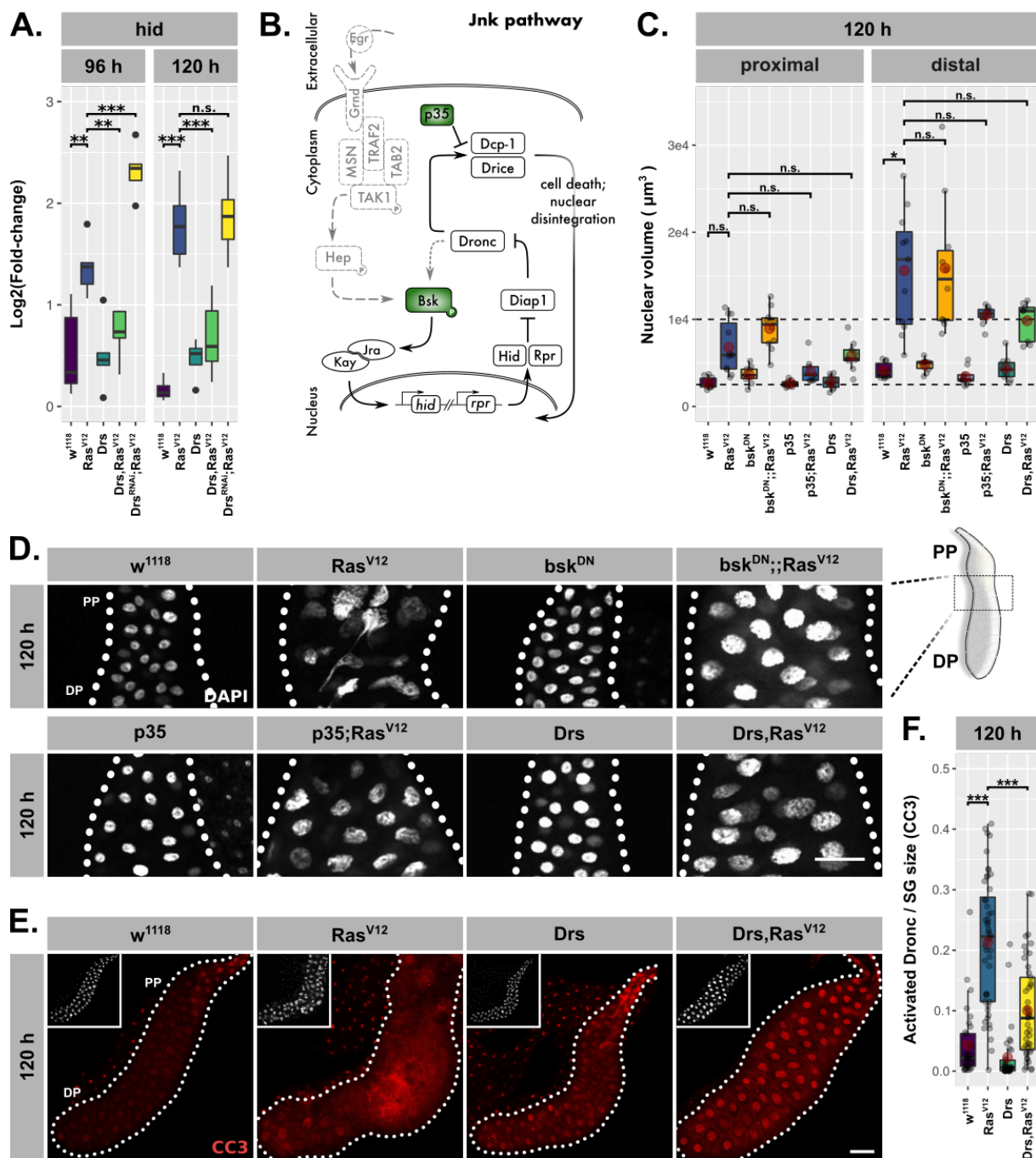
1001

1002

1003

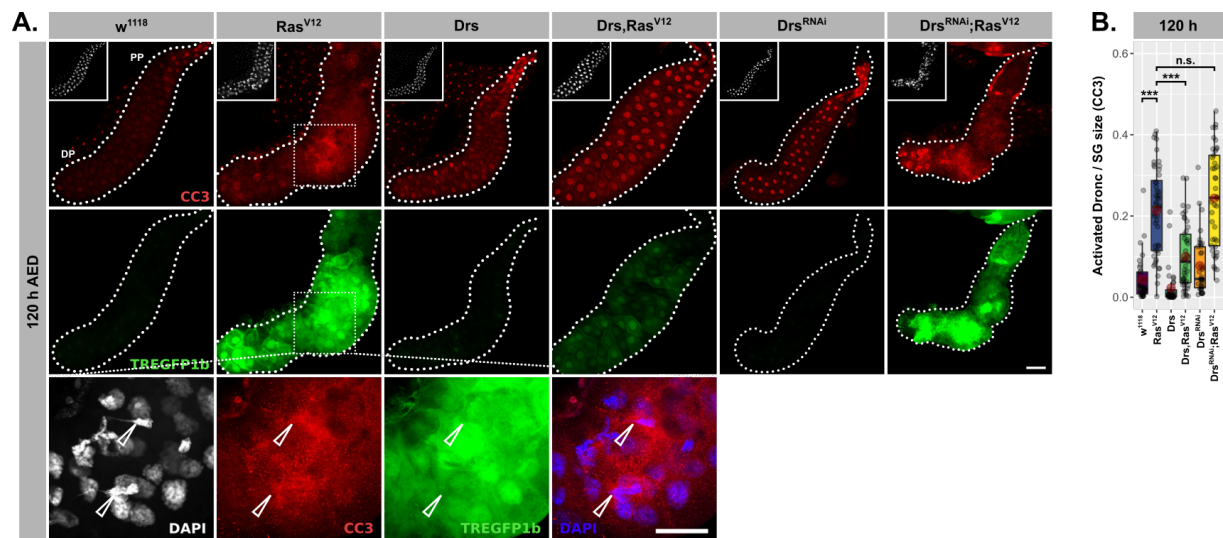
**Supplemental Figure 5.** (A.) DrsGFP reporter (green) and Hemese antibody (red) used to detect endogenous Drs expression and attached hemocytes. Expression of Drs and JNK-target genes as measured by qPCR ( $\log_2$ -transformed; normalized to *Rpl32* expression) in *Ras<sup>V12</sup>*-glands (B.) with and without inhibited JNK-pathway at 96 h AED, (C.) with and without Drs overexpression at 96 h AED and (D.) with and without Drs overexpression at 120 h AED. *Ras<sup>V12</sup>*-glands with in- (Drs) or decreased (*Drs<sup>RNAi</sup>*) Drs expression (E.) including TREGFP1b

1004 reporter (green) used to detect JNK-dependent transcriptional activation and (F.) corresponding quantifications of  
1005 reporter signal normalized for SG size. *Ras<sup>V12</sup>*-glands with in- (Drs) or decreased (Drs<sup>RNAi</sup>) Drs expression (G.)  
1006 stained for activated basket with a phosphorylation sensitive antibody (pBsk) and (H.) corresponding  
1007 quantifications of detected signal normalized for SG size. Insets: (A./E./G.) DAPI. Scalebars: (A./E./G.) 100  $\mu$ m.  
1008 Boxplots in (B./C./D./F./H.): lower/upper hinges indicate 1<sup>st</sup>/3<sup>rd</sup> quartiles, whisker lengths equal 1.5\*IQR, red  
1009 circle and bar represent mean and median. Significance evaluated by Student's t-tests (\*\* $p < 0.001$ , \*\* $p < 0.01$ , \*  
1010  $p < 0.05$ , *n.s.*  $p \geq 0.05$ ). MMP1 and MMP2 expression in (C./D.) for *w<sup>1118</sup>*- and *Ras<sup>V12</sup>*-glands also shown in Fig4D.  
1011 Hid expression in (C./D.) also presented in Fig6A. Images for *w<sup>1118</sup> / Ras<sup>V12</sup> / Drs / Drs,Ras<sup>V12</sup>* in (E./G.) also  
1012 presented in Fig5E./F.  
1013



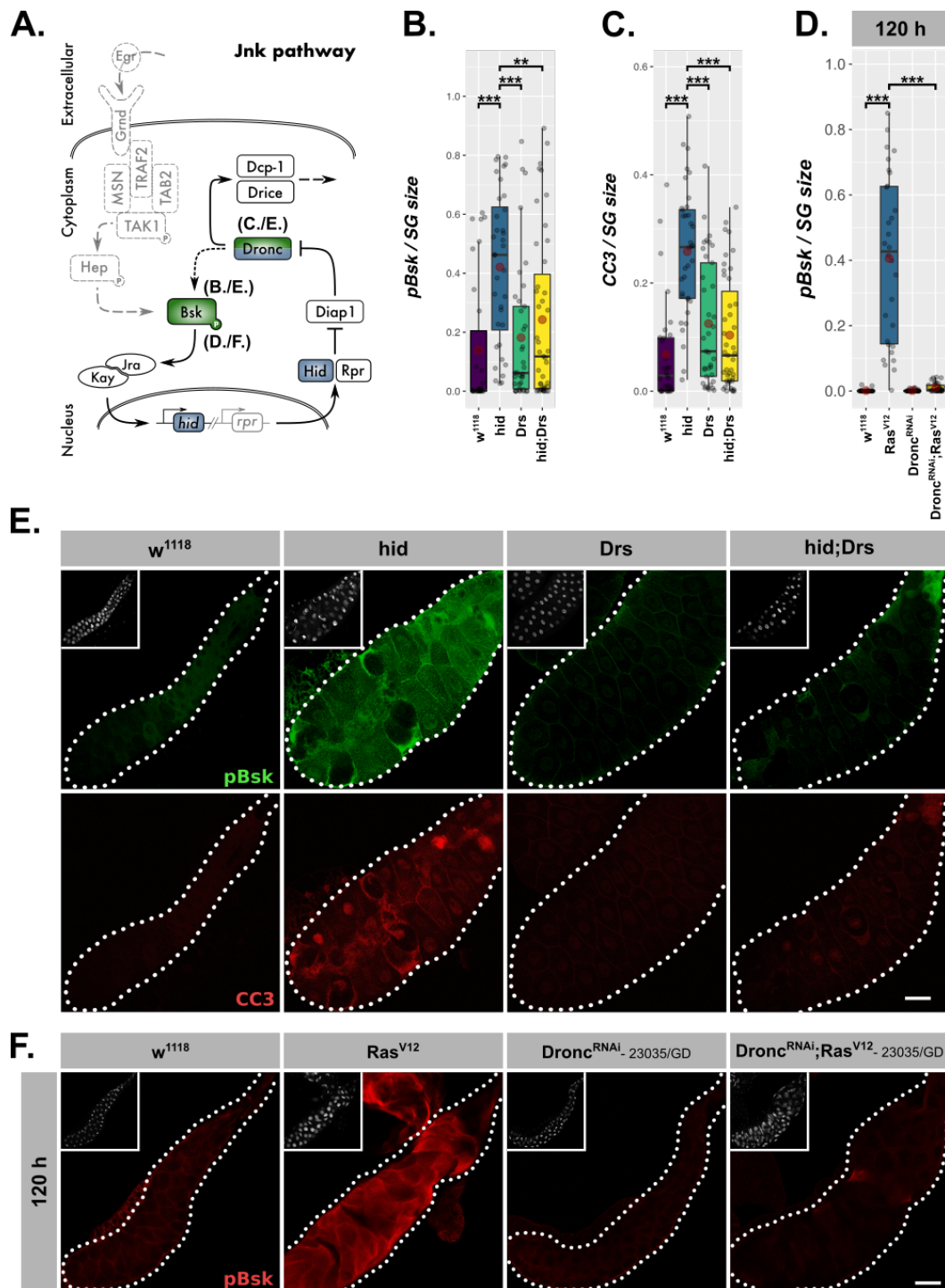
1014  
1015  
1016  
1017  
1018  
1019  
1020  
1021  
1022  
1023  
1024  
1025

**Figure 6. Drs inhibits programmed cell death** (A.) *Hid* expression as measured by qPCR and plotted as  $\text{log}_2$ -transformed values normalized to *Rpl32*-expression in  $\text{Ras}^{V12}$ -glands with in- (*Drs*) or decreased ( $\text{Drs}^{\text{RNAi}}$ ) *Drs* expression. (B.) Schematic representation of the JNK-pathway including levels of employed interference (green). (C.) Nuclear volumina derived from z-stacks of DAPI-stained SGs and averaged per gland at 96 h and 120 h AED. (D.) DAPI stained (white) SG nuclei to indicate nuclear size and disintegration.  $\text{Ras}^{V12}$ -glands with in- (*Drs*) or decreased ( $\text{Drs}^{\text{RNAi}}$ ) *Drs* expression (E.) stained with anti-CC3-antibody to detect Dronc activation (red) and (F.) corresponding quantifications of detected signal normalized for SG size. Insets in (E.) show DAPI and scalebars in (D./E.) represent 100  $\mu\text{m}$ . Lower/upper hinges of boxplots in (A./C./F.) indicate 1<sup>st</sup>/3<sup>rd</sup> quartiles, whisker lengths equal 1.5\*IQR, red circle and bar represent mean and median. Significance evaluated by Student's t-tests (\*\*\*)  $p < 0.001$ ).



1026  
1027  
1028  
1029  
1030  
1031  
1032  
1033  
1034  
1035

**Supplemental Figure 6.** (A.) *Ras<sup>V12</sup>*-glands with in- (*Drs*) or decreased (*Drs<sup>RNAi</sup>*) *Drs* expression stained for activated Dronc (red) via the CC3-antibody, JNK-dependent transcriptional activation via the TREGFP1b reporter (green) and nuclei size and disintegration via DAPI (white). Arrows in magnified images point towards strong CC3-staining correlating with disintegrating nuclei. Insets represent DAPI staining and scalebars correspond to 100  $\mu$ m. (B.) Quantifications of CC3-staining per gland normalized for SG size in *Ras<sup>V12</sup>*-glands with in- (*Drs*) or decreased (*Drs<sup>RNAi</sup>*) *Drs* expression. Lower/upper hinges of boxplots in (A./C./F.) indicate 1<sup>st</sup>/3<sup>rd</sup> quartiles, whisker lengths equal 1.5\*IQR, red circle and bar represent mean and median. Significance evaluated by Student's t-tests (\*\*\*)  $p < 0.001$ , \*\*  $p < 0.01$ , \*  $p < 0.05$ , n.s.  $p \geq 0.05$ ).



1036

1037

1038

1039

1040

1041

1042

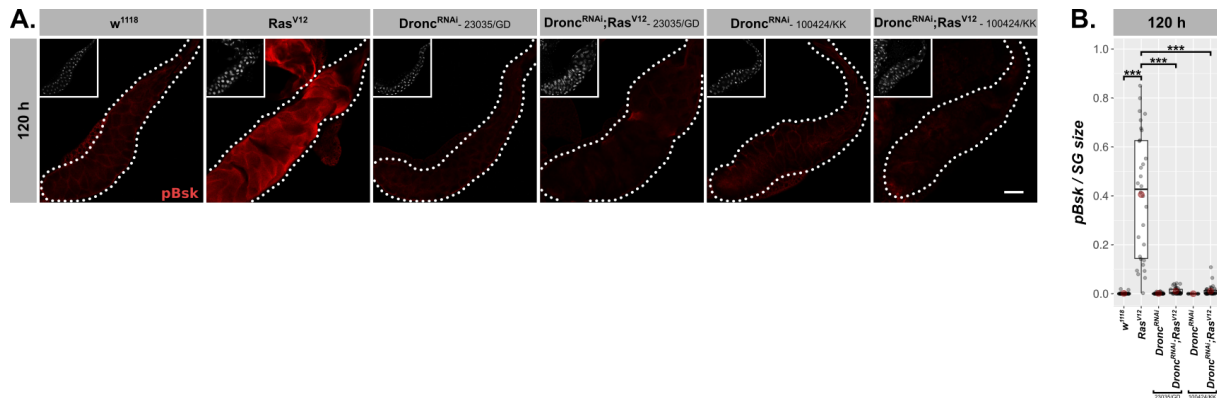
1043

1044

1045

**Figure 7. Drs inhibits the JNK-feedback loop** (A.) Schematic representation of the JNK-feedback loop including levels of interference (blue) and employed read-outs of its activity (green). *hid*-overexpressing glands with or without coexpressed Drs were quantified for (B.) activated basket via a phosphorylation sensitive antibody and (C.) activated Dronc via the CC3-antibody. (D.) Activated basket (pBsk) was quantified and normalized to SG size. (E.) *Ras<sup>V12</sup>*-glands with or without Drs-coexpression were stained for activated basket (green) and activated Dronc (red). (F.) Activated basket was detected in *Ras<sup>V12</sup>*-glands with or without Dronc-knock-down. Insets: (E./F.) DAPI. Scalebars: (E./F.) 100  $\mu$ m. Boxplots in (B./C./D.): lower/upper hinges indicate 1<sup>st</sup>/3<sup>rd</sup> quartiles, whisker lengths equal 1.5\*IQR, red circle and bar represent mean and median. Significance evaluated by Student's t-tests (\*\*\*)  $p < 0.001$ , \*\*  $p < 0.01$ , \*  $p < 0.05$ , n.s.  $p \geq 0.05$ ).





1046

1047

1048

1049

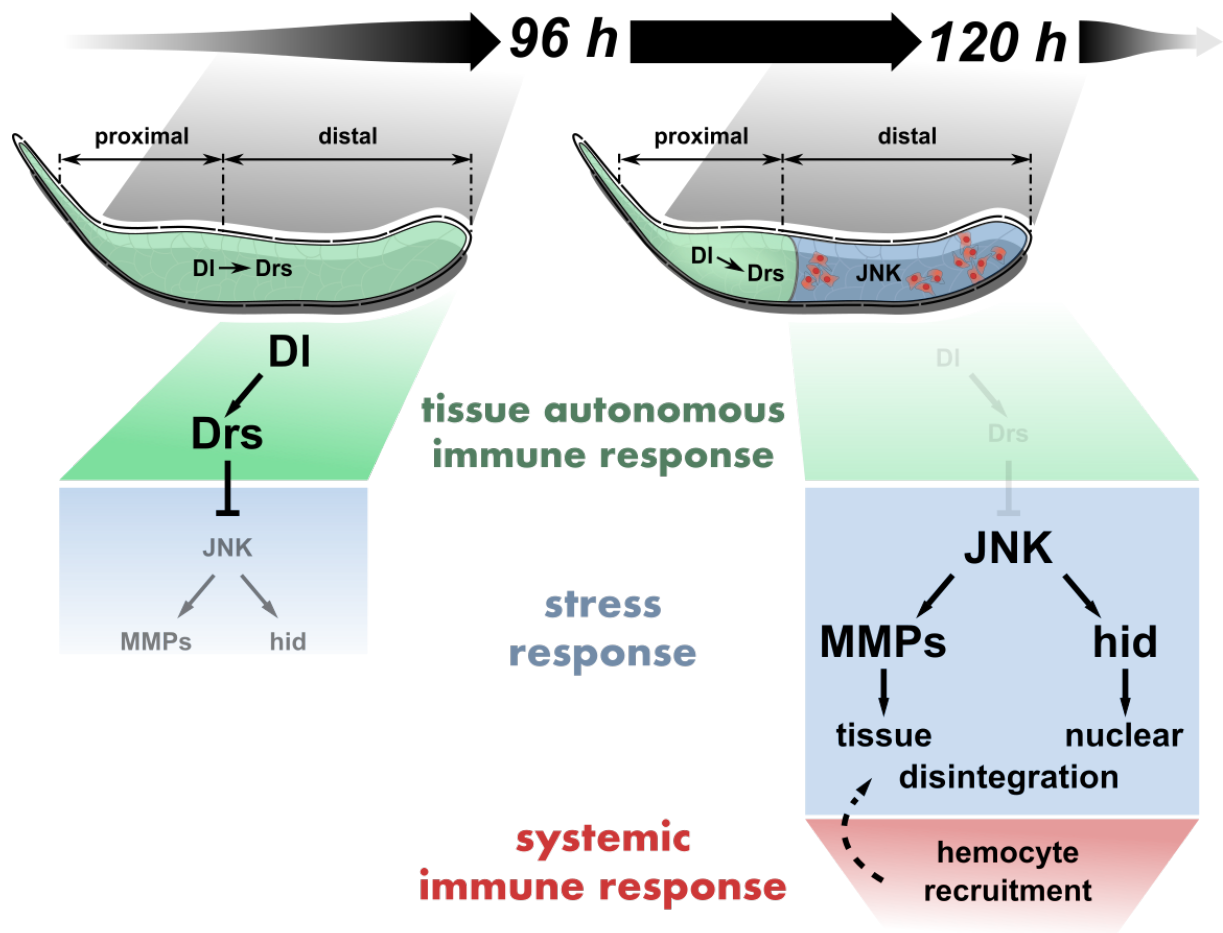
1050

1051

1052

1053

**Supplemental Figure 7.** (A.) *Ras<sup>V12</sup>*-glands with or without Dronc-knock-down were stained for activated basket with a phosphorylation sensitive antibody at 120 h AED and (B.) the signal was quantified per SG and normalized for its size. Results for both RNAi-lines used, 23035/GD and 100424/KK, were consistent. Insets in (A.) show DAPI and scalebar represents 100  $\mu$ m. Lower/upper hinges of boxplots in (B.) indicate 1<sup>st</sup>/3<sup>rd</sup> quartiles, whisker lengths equal 1.5\*IQR, red circle and bar represent mean and median. Significance evaluated by Student's t-tests (\*\*\*)  $p < 0.001$ , \*\*  $p < 0.01$ , \*  $p < 0.05$ , n.s.  $p \geq 0.05$ ).



1054

1055 **Figure 8. Tissue-autonomous antagonizes systemic immune response via JNK-inhibition in *Ras<sup>V12</sup>*-glands**

1056 Dorsal-mediated *Drs* expression inhibits JNK activation in the entire *Ras<sup>V12</sup>*-gland until 96 h AED. At 120 h AED,

1057 Dorsal and thus *Drs* expression is reduced to the PP, derepressing full JNK-activation in the DP. Consequently,

1058 JNK-dependent expression of *hid* and *MMP2* stimulates nuclear and tissue disintegration, which eventually leads

1059 to the interference with tissue growth and integrity by the systemic immune response.